Accepted Manuscript

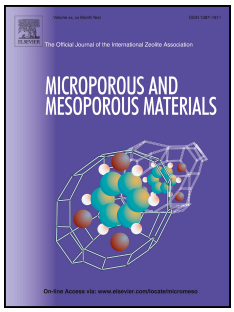

Complex investigation of charge storage behavior of microporous carbon synthesized by zeolite template

Marija Stojmenović, Milica Vujković, Ljiljana Matović, Jugoslav Krstić, Anđelka Đukić, Vladimir Dodevski, Sanja M. Živković, Slavko Mentus

PII: S1387-1811(16)30055-5

DOI: 10.1016/j.micromeso.2016.03.029

Reference: MICMAT 7643

To appear in: *Microporous and Mesoporous Materials*

Received Date: 2 November 2015

Revised Date: 25 February 2016

Accepted Date: 21 March 2016

Please cite this article as: M. Stojmenović, M. Vujković, L. Matović, J. Krstić, A. Đukić, V. Dodevski, S.M. Živković, S. Mentus, Complex investigation of charge storage behavior of microporous carbon synthesized by zeolite template, *Microporous and Mesoporous Materials* (2016), doi: 10.1016/j.micromeso.2016.03.029.

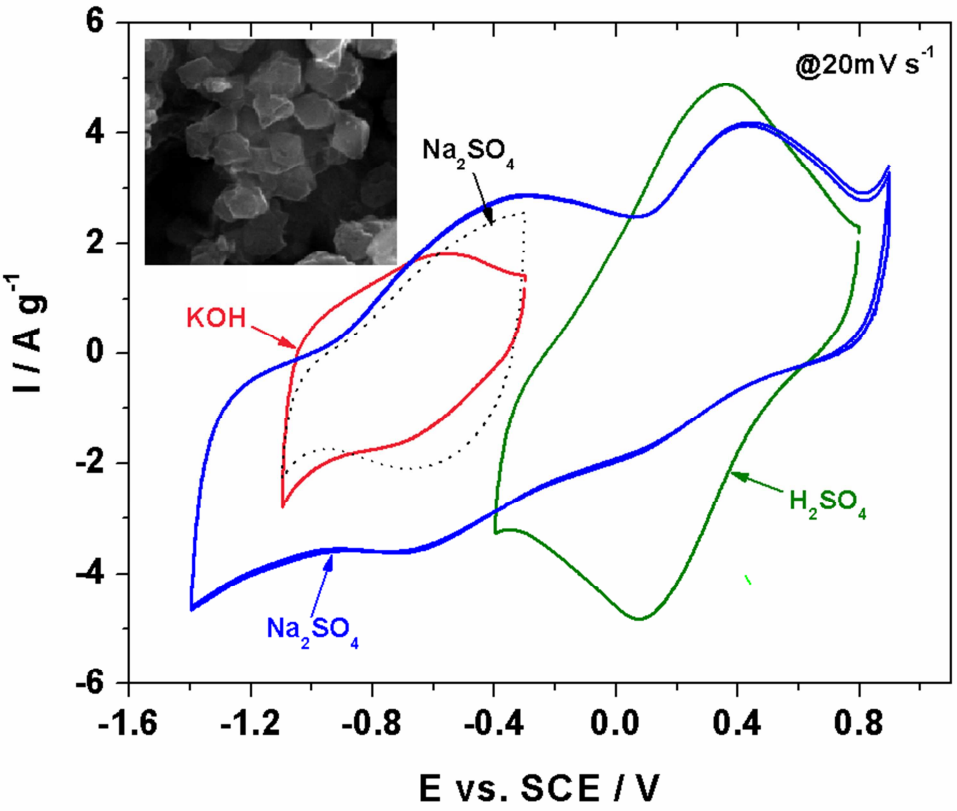

Complex investigation of charge storage behavior of microporous carbon synthesized by zeolite template

Marija Stojmenović[a,*], Milica Vujković[b], Ljiljana Matović[a], Jugoslav Krstić[c], Anđelka Đukić[a], Vladimir Dodevski[a], Sanja M. Živković[a], Slavko Mentus[b,d]

[a]*Institute of Nuclear Sciences "Vinča", Mike Petrovica Alasa 12–14, 11001 Belgrade, University of Belgrade, Serbia*

[b]*University of Belgrade, Faculty of Physical Chemistry, Studentski trg 12–16, 11158 Belgrade, Serbia*

[c]*University of Belgrade, Institute of Chemistry, Technology and Metallurgy, Department of Catalysis and Chemical Engineering, Njegoševa 12,11000 Belgrade, Serbia*

[d]*Serbian Academy of Sciences and Arts, Knez Mihajlova 35, 11000 Belgrade, Serbia*

***Corresponding author:**

Marija Stojmenović, PhD

University of Belgrade, Institute of Nuclear Sciences "Vinča"

Mike Petrovića–Alasa 12–14, 11001 Belgrade, Serbia

E–mail: mpusevac@vinca.rs

Phone: +381 11 340 8860

Fax: +381 11 340 8224

Abstract

Microporous zeolite templated carbon (ZTC) was synthesized by impregnation method using zeolite Y (Na–form) as a template, and furfuryl alcohol as a carbon precursor. The characterization was carried out by X-ray diffractometry, Raman spectroscopy, scanning electron microscopy, nitrogen physisorption, elemental analysis and electrochemical methods. Physisorption measurements evidenced high micropore volume of obtained material (~ 0.43 cm^3 g^{-1}). The charge storage ability in aqueous KOH, H_2SO_4 and Na_2SO_4 solutions was systematically studied by cyclic voltammetry, galvanostatic charging/discharging and complex impedance measurements. Specific coulombic capacitance, the hydrogen storage, H–ZTC bonding and relaxation time of adsorption were found to be dependent on the type of electrolyte. Neutral Na_2SO_4 aqueous solution was found to be the best for supercapacitor application, thanks to: i) the highest available voltage window ii) lowest corrosion and iii) highest capacitance amounting to 123 F g^{-1} at 1 A g^{-1}.

Keywords: microporous carbon, zeolite template, pseudocapacitor, aqueous neutral electrolyte, hydrogen storage

1. Introduction

Since Chmiola et al. [1, 2] found anomalous increase of double layer capacitance of porous carbons when pore diameter became less than the diameter of solvated electrolyte ions, an expansion of investigation of microporous carbon materials as electrochemical supercapacitors happened [3–9]. The importance of micropores (diameter below 2 nm) in charge storage was also confirmed [6, 10]. The oxygen functional groups, usually presented in the micropores of carbon

surface, boosted the capacitance either through the faradaic reactions [11, 12] or through the enhancement of wettability [9, 11, 13]. The influence of mesopores was also emphasized, due to their role as the transporting channels for adsorbed ions [14, 15].

Different methods of synthesis of carbon materials were applied in order to adapt the porosity of carbon materials [16–20]. The templated carbonization method belongs to the most elegant methods [21–27]. Mesoporous silicates and microporous zeolites were the most commonly used as templates [28]. The first attempt to obtain carbon obeying the zeolite pore structure was described by Kyotani et al [29]. By introducing the furfuryl alcohol into the cannels of zeolite Y, followed by polymerization and carbonization, these authors obtained microporous carbons with very high specific surface area of 1140 $m^2\ g^{-1}$ [29, 30] and 2260 $m^2\ g^{-1}$ [31], but with a significant fraction of mesopores, as well. Many authors followed this synthesis method [32–35]. Kyotani's group [35] succeeded to prepare microporous carbon whose structure completely reflected the one of original zeolite. For the porous carbon obtained, abbreviated as ZTC, very high specific surface area of 3600 $m^2\ g^{-1}$ and micropore volume up to 1.5 $cm^3\ g^{-1}$, with a negligible mesopore fraction were reported [36]. The theoretical prediction of specific surface area for carbon materials, derived under assumption that all C–atoms are spread within an idealized graphene layer structure [37] amounts, however to 2630 $m^2\ g^{-1}$. Highly structure ordered ZTC's were successfully synthesized using only small group of zeolites as hard templates: Y(X) zeolite [35, 38, 39], zeolite β [38, 40] and EMT [41]. It was shown that various carbonaceous materials, ranging from pure microporous carbons (highly long–range ordering structure) to carbons with different fractions of mesopores (poor ordering structure), can be obtained by an adequate selection of the synthesis procedure [36].

In comparison to activated carbons [42] and carbide derived carbons (CDS) [43, 44] the investigations of zeolite–templated carbons (ZTC) as supercapacitors are much less numerous. High charge storage capability in both aqueous [45–49] and organic [46, 50, 51] electrolyte solutions were found for high surface area ZTC's. Kajds et al. [47] reported high charge storage pseudocapacitance of zeolite Y–templated carbon amounting to 300 $F\ g^{-1}$ in H_2SO_4 solution. For N–containing microporous zeolite–templated carbon, with specific surface of 1680 $m^2\ g^{-1}$, specific capacitance of 340 $F\ g^{-1}$ at 0.1 $A\ g^{-1}$ in H_2SO_4 was measured [45]. The microporous carbon with created fraction of mesopores, prepared by using a zeolite 13X template, displayed also the high capacitance of 259 $F\ g^{-1}$ in 6 mol dm^{-3} KOH and 176 $F\ g^{-1}$ in organic electrolyte, at

the current density of 0.25 A g^{-1} [46]. The combined effects of N– and O– containing surface functional groups were considered in explanation of specific coulombic capacity in various solutions [45, 46]. The carbon texture having the pure zeolite structural regularity and a very high surface area of 3689 m^2 g^{-1}, obtained by two-step impregnation method, according to Itoi et al. [49], displayed also an extremely high capacitance of ~ 470 F g^{-1} at 1 A g^{-1}, in H_2SO_4 solution. This specific capacitance is the highest ever reported among carbon materials.

Electrochemical oxidation of ZTC was found to be an effective way to generate a large number of surface oxygen groups [49, 52].

The solutions of KOH and H_2SO_4 are the most commonly used aqueous electrolytes in carbon capacitors examination. Low decomposition voltage of water in comparison to organic electrolytes is obstacle for commercialization [53–55], however, better environmental friendliness, low cost and simpler handling are significant advantages of aqueous electrolytes. Recently, neutral sulphate solution was demonstrated as the best choice of aqueous electrolytes, providing higher potential window (even up to 2.4 V) [54–56] and slower corrosion than both acidic and alkaline solutions [53]. However, better conductivity [57] and pseudofaradaic (surface) reactions enable somewhat higher capacitances in acidic and alkaline solutions [58].

To contribute to the knowledge of carbon supercapacitor behavior in aqueous solutions, we used zeolite Y (Na–form, SiO_2/Al_2O_3 = 5.6) as a template and furfuryl alcohol (FA) as a carbon precursor, to prepare preferably microporous ZTC, with specific surface area ranging 1000 m^2 g^{-1}. It's charge storage behavior was examined in various aqueous electrolytes: 6 mol dm^{-3} KOH, 0.5 mol dm^{-3} Na_2SO_4, and 0.5 mol dm^{-3} H_2SO_4. The difference in capacity was correlated to surface texture and difference in surface functionalities.

By using the less surface developed ZTC, one of the concern of this work was to provide the higher potential stability window compared to that obtained with others highly ordered ZTCs [45, 46, 49]. We also intended to prove whether the ZTC obtained by the simplified, one step, soaked polymer carbonization procedure, may prove a satisfactory high capacitance, having in mind that the capacitance is not uniquely correlated to the specific surface area [8, 9].

2. Experimental

2.1. Synthesis of ZTC sample

Zeolite templated carbon (ZTC) was synthesized using zeolite Y (Na–form, SiO_2/Al_2O_3 = 5.6) according to the procedure previously descibed by Z. Ma et al. [36]. 10 ml of furfuryl alcohol (FA) was added into the flask containg 2.5 g of zeolite Y under inert atmosphere. The polymerization of FA was carried out by heating the suspension at 80 ºC for 24 h and then at 150 ºC for 8 h under N_2 flows. The resultant zeolite/polyfurfuryl alcohol (PFA) composite was heat–treated in a vertical quartz reactor under an N_2 flow at a heating rate of 5 ºC/min up to 800 ºC and treated isothermally at this temperature for 4 h. The prepared zeolite/carbon composite was treated with 46 % HF for 24 h to dissolve zeolite matrix, and upon separation of carbon from the solvent by filtration and washing to disappearance of mineral traces, it was subsequently dried at 120 ºC in air for 3 h.

2.2. Physico–chemical charaterization

Textural characteristics of ZTC powder were determined by the nitrogen sorption method at -196 ^{o}C using a Sorptomatic 1990 Thermo Finnigan. Before measurement, the sample was degassed for 4 h at room temperature and for 18 h at 350 ^{o}C under vacuum. The resulting N_2 adsorption isotherms were analyzed by Software ADP Version 5.17 CE Instruments. According to the recommendations for carbon materials [59], specific surface area (S_{BET}) was calculated using BET (Brunauer, Emmet, Teller) equation from the best linear fit in the region $p/p_0<0.01$ (p and p_0 represent the equilibrium and saturation pressures of nitrogen at fixed temperature). To determine microporosity, several methods were applied, including Dubinine–Radushkevich [60], Horvath–Kawazoe (HK) [61] and α_S–plot methods [62]. For α_S–plot method, standard isotherm proposed by Kruk at al. [63] was applied. Mesopore surface area, $S_{meso\text{-}\alpha s}$, was also evaluated using α_S–method, while the mesopore volume, $V_{meso\text{-}BJH}$ and mesopore size distribution was estimated by the Barrett, Joyner and Halenda (BJH) method [64].

XRPD measurement was carried out using Ultima IV Rigaku diffractometer, equipped with Cu $K_{\alpha 1,2}$ radiation source. The voltage of 40.0 kV and a current of 40.0 mA were used. A continuous scan mode in the range of 4–70 º2θ, was performed with a step size of 0.02 º and scan rate of 2 º/min.

By a diode pumped solid state high–brightness laser (532 nm), excited Raman spectra was collected in the spectral range 600–1800 cm^{-1} on a DXR Raman microscope (Thermo

Scientific, USA) equipped with an Olympus optical microscope and a CCD detector. Analysis of the scattered light was made by the spectrograph with a grating 900 lines/mm.

The microstructural and morphological analysis was performed by scanning electron microscope (SEM) VEGA TS 5130MM (Tescan SEM) The chemical analysis was performed by an Energy Dispersive Spectrometer (EDS) at invasive electron energy of 30 keV by means of QX 2000S (Company Oxford Microanalysis Group), which was connected to the device VEGA TS 5130MM (Tescan SEM).

The elemental analysis was performed by an inductively coupled plasma–atomic emission spectrometry (ICP–AES) on an ICP spectrometer Spectro Flame (Spectro Analytical Instruments, Germany). The sample was prepared as follows: to an amount of 53.7 mg of sample in a Teflon vessel 5 cm^3 HNO_3 (65 %) + 2 cm^3 H_2SO_4 was added. After 10 min vessel was closed and put into microwave oven, together with the blank solution. The microwave digestion was performed at 200^oC for 45min. After cooling, the sample solution was transferred into 25 cm^3 calibrated flask and diluted to its volume with deionized water. The ICP–AES chemical analysis was carried to check the difference between nominal and final composition of solutions.

X-ray photoelectron spectroscopy (XPS) measurements were carried out on a SPECS customized UHV surface analysis system containing dual anode Al/Ag monochromatic source, PHOIBOS 100 spectrometer for energy analysis, electron flood gun and sputter ion gun. XPS spectra were obtained using monochromatic AlKα excitation source (1486.74 eV) in FAT 40 mode. The energy step size was 0.1 eV. The spectra analysis was determined using Shirley background subtraction. The best fits of C1s were obtained by applying the Gaussian-Lorentzian function (70:30) for all peaks with the exception of one positioned at 291.3 eV, which is wider than others component peaks. The Gaussian-Lorentzian function (30:70) was used for fitting the 291.3 eV peak as well as for all O1s component peaks.

2.3 Electrode preparation and electrochemical measurements

Working electrode was prepared by mixing ZTC, carbon black (Vulcan XC72) and poly(vinylidene fluoride) (PVDF) binder in the weight ratio 80:10:10. This mixture was suspended in N–methyl–2–pyrollidone, homogenized in an ultrasonic bath for 0.5 h and then a part of this slurry was transferred onto the glassy carbon disc. By drying in vacuum oven at 130 ^{o} C for several hours, pyrollidone was removed. All electrochemical measurements including the

cyclic voltammetry (CV), galvanostatic measurements and impedance were done in a three–electrode electrochemical cell at (25±1) ºC using Gamry PCI4/750 potentiostat/galvanostat, with wide Pt foil as a counter electrode and a saturated calomel electrode (SCE) as a reference electrode. The electrolytic solutions were 6 mol dm^{-3} KOH, 0.5 mol dm^{-3} Na_2SO_4 and 0.5 mol dm^{-3} H_2SO_4. Since preliminary CV experiments showed that there are no differences in the capacitance performance in air and in N_2 atmosphere, presented measurements were carried out in the electrolytes equilibrated with air. The impedance measurements were conducted at various potentials by applying AC voltage amplitude of 10 mV in the frequency range from 10 mHz to 100 kHz.

The specific capacitance, C (F g^{-1}) obtained from CV results, was evaluated by the integration of the area under charge/discharge CV curves according to the equation 1:

$$C = (\int I \cdot V \cdot dV) / (m \cdot \nu \cdot \Delta V) \quad (1)$$

where I is the measured current response, V is the potential, m is the mass of electroactive ZTC layer on the electrode disk, ν is the applied scan rate and ΔV is the used potential window.

3. Results and discussion

3.1. Characterization of ZTC sample

This section presents the results physico−chemical characterization of ZTC.

3.1.1. N_2–physisorption measurements

The nitrogen adsorption/desorption isotherm measured at -196 ^oC, is shown on Fig. 1a, while the corresponding calculated textural parameters are presented on Table 1.

It is worth mentioning that the isotherm was measured under conditions different from routine measurements, as discussed below.

Having in mind IUPAC classification [65], the isotherm presented in Fig. 1a is similar to BET isotherm type I, characteristic of microporous samples. High adsorption volume in a short p/p_0 <0.1 region, confirms highly developed microporosity, like to many other zeolite−templated carbons [36, 35−39]. However, the existence of the hysteresis loop in almost entire region of

relative pressures, including that below 0.4 p/p_0, indicates uncommon behavior, although the loop can undoubtedly be noticed only under higher magnification (insert in Fig. 1a). The hysteresis in the region of relative pressure range $p/p_0 > 0.4$ is otherwise not uncommon, in fact it expectedly occurs in most of the materials characterized by nitrogen physisorption. The existence of loop in this region indicates the presence of pore system inside the particles (intraparticles porosity) and/or voids between the weakly bound particle agglomerates (interparticles porosity). According to the theory, the closure point of hysteresis loop depends on the nature of the gas and for nitrogen it is expected at $p/p_0 \approx 0.42$ [59, 65]. However, in the range $p/p_0 < 0.4$ hysteresis is less common (sometimes called low pressure hysteresis−LHP), and was reported preferably for microporous materials, e.g. zeolites or carbons [36, 66-68]. The literature explanations for LHP are very different, and among them, the most common ones include: i) a flexible transition in the matrix structure upon gas uptake; ii) an irreversible intercalation of adsorptive molecules in pore structures of molecular dimensions and distortion of the porous material which may lead to the rearrangement of adsorbed molecules; iii) a lack of adsorbent/adsorbent equilibrium during the experiment and iv) an insufficient sample degassing [67-69].

Although this was not the main topics of the present paper, due to the uncommon desorption branch of the adsorption isotherm, we tested the last two of above mentioned explanations of LPH. As already presented in the experimental section, the synthesis procedure we used followed that published by Ma et al [36]. These authors presented the nitrogen isotherm of appropriate ZTC sample, denoted PFA8 in Fig. 6 [36], which displayed significant slope in the region of relative pressures 0.1−0.9 and more pronounced hysteresis, which relates to the low pressure region ($p/p0 < 0.4$), too. Our initial measurements, conducted at common equilibrium times and pressure deviations (used otherwise in routine measurements), resulted indeed in an isotherm similar to the one shown in the paper by Ma et al [36]. In order to reveal probable influence of the degassing pretreatment procedure on LPH appearance, we varied maximum degassing temperature (T_{max}) and holding time (t_{max}) on T_{max}. This enabled us to detect that the heating treatment at low temperature, less than 110 ºC, especially in combination with short degassing time (t_{max}< 10 h), leads to a significant reduction of textural parameters (V_{ads}, V_{mic} and S_{BET}), compared to those presented in Table 1. This indicated suppressed access to nitrogen molecules, due to the blocking effect of the preadsorbed molecules on the ZTC surface. At the

same time, at T_{max} < 110 ºC and t_{max}< 10 h, the shape of the isotherm and hysteresis appearance remained qualitatively unaffected.

The rise in both degassing temperature and heating time, above 350 ºC and 18 h, respectively, caused gradual change of the calculated textural parameters. The equilibrium time and pressure deviation were measured for pretreatment conditions T_{max}= 350 ºC and t_{max}= 18 h, using several pairs p_{equ}–t_{equ}, in each p/p_o sector separately, to maximize total analysis time. The experiments finished with total analysis time close to 48 h (i.e., more than 2.6 times longer in comparison to the routine equilibrium parameter measurements). The equilibrium parameters became close to the ones presented in Table 1, while the shape of the isotherm remained the same as that published by Ma et al. [36], i.e. with wide open hysteresis in the entire p/p_0 region, as one may see in Fig.1.

These results can be summarized as follows. The more demanding value of equilibrium pressure deviation and the increase in equilibrium time, even 5 times higher than used in routine analysis, in the region p/p_0 < 0.1, did not affect the resulting surface parameters. This is obviously from the value V_{mic} and S_{BET}, which practically do not change on equilibration time prolongation. On the other hand, in the sector p/p_0 > 0.2 more demanding value of equilibrium pressure deviation and prolonged equilibrium time affect the shape of isotherm, decreasing its slope and making adsorption–desorption hysteresis substantively narrower.

Although we did not success to obtain the isotherm lacking in LPH, it is obvious that longer equilibrium time reduces the LPH, as well as the hysteresis observed above p/p_0 ~ 0.4. This supports the idea of Reichenbach et al. [69], who stated that the reason of LPH can be found in "extremely slow gas uptake by the narrow nanopore system, failing to equilibrate within experimental time scales". Further analysis of the texture of ZTC sample will be made based on the results presented in Table 1.

It is not surprising that the obtained value of S_{BET} exceeds 1000 m^2 g^{-1}. However it seems this value is significantly overestimated, since capillary condensation in the micropores begins before the formation of N_2 monolayer, what in general corrupts the assessment of SSA by means of BET equation (as we already noted in Introduction section, sometimes it is larger than the theoretical value). Therefore, we used α_s–plot method and found significantly lower value of SSA, close to 500 m^2 g^{-1}. This means that the amount of nitrogen packed within an adsorbed monolayer is twice as small as estimated by BET equation. Since various methods (α_s–plot

methods, DR–method and HK method) gave mutually comparable, high values of micropore volume of ZTC, in the range of 0.4 to 0.45 cm^3 g^{-1}, we concluded that the sample is dominantly microporous. Also, pore size distribution (PSD) of ZTC in the micropore region, obtained by the Horvath–Kawazoe (HK) method (Fig. 1b), shows a sharp peak centered at about 0.51 nm, which corresponds to the width of the filled zeolite channel [70], and confirms that capillary condensation takes place far ahead of BET region.

Specific surface area of ZTC we determined is relatively low compared to the highly microporous materials prepared from the same reactants, furfural alcohol and zeolite Y, but via two–step impregnation process [36]. This indicates that during synthesis we did not achieve complete filling of zeolite channels, causing an extent of mesoporosity. The fraction of specific surface area related to mesopores, $S_{meso\text{-}\alpha_s}$, which includes the external surface area, contributes about 10 % to the total specific surface area. For mesopore size distribution, calculated according to BJH method, no prevalent pore diameter was found. Still, the role of mesopores in carbon materials, together with micropores, is very important in charge storage ability [14, 15].

3.1.2 Structural characterization and elemental composition

The results of structural characterization of sample (X-ray diffraction analysis and Raman spectroscopy), that has already known for such type of zeolite-templated carbons, were analyzed by using references [71-75] and shown in Supplementary Information. The elemental composition of the ZTC powder obtained by both energy–dispersive X–ray (EDX) and inductively coupled plasma–atomic emission spectrometry (ICP–AES) analysis was presented in the Supplementary Information, too.

3.1.3. Morphology

Fig. 1c,d shows the SEM images of ZTC powder under two different magnifications. At a first glance, ZTC obeys the morphology of zeolite Y [36, 72]. The particles have quite uniform sizes and irregular shapes, with somewhat smooth surfaces. Some roughness on the surface originates probably from the excess of carbon deposited at the outer surface of zeolite particles [72]. Furthermore, the ZTC particles of uniform size of about 0.3 µm are smaller than those of the template. This is due to the shrinkage of zeolite particles, as well as shrinkage of the carbon itself, upon high temperature carbonization. Such collapse of the zeolite/carbon particles, after

removal of template, can produce the fracture causing the decrease of micropore fraction, and the creation of slit like mesopores [73].

3.1.4. Analysis of surface oxygen groups by XPS

Surface oxygen-containing groups of ZTC were analyzed by XPS. The C1s and O1s spectra of ZTC were shown in Fig. 2. The C1s spectrum was deconvoluted into five individual peaks positioned at 284.6eV, 286.5 eV, 287.7 eV, 289.2 eV and 291.3 eV (Fig. S.1a) corresponding to sp^2 carbon, carbon in alcohol or ether groups (C-OH and/or C-O-C), carbonyl groups (C=O), carboxyl groups (OH-C=O) and shake-up satellite peaks due to π-π^* transitions in aromatic rings, respectively [76]. The ratio of each group was found to be 87.1%, 2%, 2.8%, 2.5% and 5.6%, respectively. The O1s spectrum was resolved in three component peaks located at 531.3 eV, 533.1 and 535.4 eV corresponding to C=O quinone groups, C-OH phenol and/or C-O-C ether groups, and chemisorbed oxygen and/or water, respectively [76]. Their relative ratio was amounted 38.6%, 42.9% and 18.4%, respectively.

3.2. Electrochemical investigation

3.2.1. Charge storage by cyclic voltammetry

The charge storage behavior of ZTC was examined in three different aqueous electrolytes: 6 mol dm^{-3} KOH, 0.5 mol dm^{-3} Na_2SO_4 and 0.5 mol dm^{-3} H_2SO_4. Corresponding cyclovoltammograms, measured at different scan rates, were presented in Fig.3. On potendiodinamic cycling, within the potential region of water stability, in all aqueous electrolytes, ZTC behaves as a non–ideal capacitor (i.e. the CV's were non–rectangular in shape). This indicates that the charging of ZTC surface included both the formation of electrical double layer, (responsible for cathodic-anodic current distance at potentials where no redox reactions occur) as well as the pseudo–faradaic contribution of the surface functional groups (responsible for cathodic/anodic peaks).

Pseudo–capacitance behavior of ZTC, evidenced by the appearance of pairs of redox peaks, is a consequence of pseudo–faradaic reactions of the surface oxygen functional groups. Unlike some carbon materials [9], whose CV curves shape is independent on the type of electrolyte, the CV curves of ZTC are affected by the choice of electrolytic solution. Comparison of the CVs (Fig. 4a), in measured electrolytes at a common scan rate, clearly shows that pseudo–

capacitance contribution increases with the decrease of pH, following the order KOH, Na_2SO_4, H_2SO_4. Namely, small current bulge at both anodic and cathodic branch of CV's, measured in KOH, rises to well pronounced pair of redox peaks in 0.5 mol dm^{-3} H_2SO_4. Reversible redox peaks in acidic medium have been already well–documented in literature **[**3, 54, 77,78] and were attributed to the fast redox reactions of surface oxygen functional groups including reversible oxidation/reduction of quinone to hydroquinone (XPS spectra provide evidence for the presence of quinone groups at the surface of ZTC), according to the equation 2:

$$O{=}Ph{=}O + 2H^{+}{+}2e^{-} \leftrightarrow HO{-}Ph{-}OH \quad (2)$$

Andreas et al. reported [58] that the redox reactions of quinone/hydroquinone are not active in an alkaline solution due to an insufficient hydrogen concentration but these authors showed that other groups, such as pyron groups, can be activated in the solutions of high pH. Therefore, the appearance of humps in KOH (Fig. 3a) can be attributed to pyron–like functional groups. Although the same authors suggested that quinone/hydroquinone reactions are not active in neutral solutions as well, the potentiodynamic cycling of ZTC in 0.5 mol dm^{-3} Na_2SO_4 (Fig. 3b) showed opposite results. Two pair of redox peaks (positioned at –0.33 V/–0.67 V and –0.42 V/0.11 V vs. SCE for 20 mV s^{-1}) were evidenced in CV's of ZTC in Na_2SO_4 solution. Beguin et al. [54] have already reported the redox activity in 0.5 mol dm^{-3} Na_2SO_4, but these authors measured one pair of redox peaks positioned at –0.1 V/ 0.1 V vs. NHE. Having in mind the CVs reported in ref. [79], it can be confirmed that both peaks of ZTC in sodium sulphate originate from two electron quinone/hydroquinone redox reaction. Even though the concentration of hydrogen ions into 0.5 mol dm^{-3} Na_2SO_4 is low, it is still sufficient to activate the charge transfer of quinone groups in two steps.

Interestingly, when the ZTC electrode was cycled in either Na_2SO_4 or KOH solution to the same vertex cathodic potential, similar charge storage capacity was obtained (Fig. 4a). It can be attributed to the similar radius of adsorbing partially desolvated K^+ and Na^+ cations as well as OH^- and SO^{2-}_4 anions [80]. Therefore, the positive–going scan contributes to the significantly pronounced redox processes even at negative potentials. The reason for that is an additional oxidation of ZTC surface which includes formation of the surface oxygen groups under anodic polarization. The differences between cathodic currents were observed, if two successive cycles

were measured in the narrow potential intervals (from –0.3 V to –1.1 V vs. SCE and from 0 V to –1.4 V vs. SCE) in Na_2SO_4, immediately after scanning in wide potential interval (from 0.9 to –1.3V vs. SCE), Fig. 4b. Namely, the CV curves, marked as dashed and dotted curves (Fig. 4b), show that the cathodic current in the first negative–going scan (3 or 6 cycle) is significantly higher when compared to that measured in the next cycle (4 or 7 cycle, respectively) due to reduction of oxygen groups formed upon previous positive–going scan.

The shape of cyclovoltammetric curves of ZTC is independent on the scan rate (Fig. 3) in each of electrolytes, indicating stable and reproducible capacitance behavior, which is also evidenced by overlapping of CV curves during first five cycles (Fig. 4a). The values of specific capacitance, calculated according to the equation 1, are shown in the Table 2. The increase in the scan rate results in the decrease of capacitance which is general characteristic of all real capacitors.

The specific capacitance in various electrolytes, observed at a common sweep rate, increases in the order: KOH<Na_2SO_4<H_2SO_4. Higher capacitance of ZTC in H_2SO_4 acidic solution than in Na_2SO_4 and especially in KOH, can be due to i) higher concentration of H_3O^+ ions in acidic electrolyte and their stronger interaction with surface oxygen atoms compared to analogous interaction of K^+ and Na^+ ions ii) better mobility and penetration of hydrated H_3O^+ ions into micropores relative to hydrated Na^+ and K^+ ions [53], iii) additional oxidation of carbon surface at positive potentials. Still, the capacity drop with the scan rate increases in the same trend, KOH<Na_2SO_4<H_2SO_4. The main reason for that behavior is the increase of the double layer participation relative to pseudocapacitance with the increase of pH. With regard to stability potential interval, the use of neutral sulphate solution allows much higher operating voltage (~2.3 V at 20 mV s^{-1}) than acidic or alkaline solution (~0.8 V and ~1.4 V, respectively, at 20 mV s^{-1}). Strong solvation of SO_4^{2-} with H_2O molecules [55], together with reversible hydrogen electrosorption, could be responsible for the shift of overvoltage of hydrogen evolution, allowing the achievement of high operating voltage.

In order to explain quantitatively the difference in the retention of measured capacitances with the increase in scan rate, we considered the redistribution of charge in the "outer" and "inner" part of carbon surface, calculated by the procedure developed by Trassati [81]. The whole amount of charge that could be stored in ZTC, calculated from the intercept of the linear plot $1/q^*$ versus $v^{1/2}$, amounted to 77 F g^{-1}, 132 F g^{-1} and 226 F g^{-1} in KOH, Na_2SO_4 and H_2SO_4,

respectively. The charge stored in the "inner" part of carbon surface, representing the difference between the whole charge and the charge stored at the "outer" surface (q_o–outer charge was calculated as intercept of linear part q vs $v^{1/2}$) amounted to 32 F g^{-1}, 63 F g^{-1} and 168 F g^{-1}. Upon cycling at high scan rates only the outer surface can be utilized for charge accumulation due to limited ability of ions to penetrate into micropores. Therefore, the capacity decrease on rising scan rate, observed in all electrolytes, follows the trend of charge accumulated in the inner part of surface, in an order KOH, Na_2SO_4, H_2SO_4.

3.2.2. H-ZTC bonding

By testing different carbon materials in various aqueous electrolytes, Beguin at al. [54] investigated the influence of pH and/or electrolyte ions radii, on the double layer capacitance, as well as on the hydrogen storage, pointing out the difficulty in understanding these processes. The situation may even be more complex when the carbon material behaves as a pseudocapacitor since the redox reactions are very sensitive to the change in pH. Incited by their publications [54, 82], we measured the dependence of hydrogen storage and H–C bonding in ZTC on the type of aqueous electrolyte solution.

The cyclic voltammograms of ZTC, in three electrode cell, with 6 mol dm^{-3} KOH, 0.5 mol dm^{-3} Na_2SO_4 and 0.5 mol dm^{-3} H_2SO_4 solutions, were also measured in an extended negative voltage interval (Fig. 5). When the negative "cut–off" potential was shifted in steps of 100 mV, in each consecutive cycle, below the onset potential of hydrogen evolution, (the vertical dashed lines indicates the approximate value of hydrogen equilibrium potential at 25 ^oC), the reduction current of hydrogen evolution was observed as well as the corresponding hump of stored hydrogen oxidation. Generally, a deep cathodic polarization of some carbon material [83-84], which leads to the water reduction, causes that evolved hydrogen adsorbs on carbon surface, whereas the anodic polarization result in the appearance of the hydrogen oxidation peak. The efficiency of this process i.e. hydrogen diffusion into carbon pores, depends not only on the type of carbon but also on the nature of the electrolyte. The more hydrogen atoms penetrate into micropores during cathodic water reduction, the higher hydrogen oxidation peak is observed.

According to the increase of anodic current of adsorbed nascent hydrogen (insets in Fig. 5) upon each enlargement of vertex cathodic potential, it can be clearly seen that the hydrogen

storage in ZTC is possible even at relatively high sweep rate of 20 mV s^{-1}. This is due to the developed ZTC microporosity. One can see that hydrogen storage capacity follows the order KOH<Na_2SO_4<H_2SO_4. The cathodic current of HER in H_2SO_4 is the highest, but the increase of anodic peak with the potential shifting below the onset potential of hydrogen evolution is almost negligible. This indicates a very poor hydrogen storage based capacity of ZTC in acidic electrolyte, at high scan rate, since hydrogen recombines quickly into the molecular hydrogen, by Tafel or Heyrovski process, rather than it incorporates into material [84]. Unlike this, HER of ZTC in neutral and alkaline solution is significantly slower, which allows hydrogen atoms to diffuse into micropores of carbon surface, even at high scan rates, and to be oxidized during anodic sweep, according to the equation ZTC–H_{ads}→ZTC + H^+ + e^-.

The peak corresponding to the oxidation of the stored hydrogen is observed at ~ –0.6 V vs. SCE in KOH and ~ +0.5 V vs. SCE in Na_2SO_4. Comparison of this voltage with the thermodynamic value of hydrogen evolution (~ –1.1 V and ~ –0.6 V vs. SCE, respectively*)* indicates a strong bonding between ZTC and incorporated hydrogen in both alkaline and neutral electrolytes. The higher overvoltage for hydrogen oxidation in Na_2SO_4 than in KOH shows the stronger ZTC–H_{ads} bond in Na_2SO_4 relative to KOH solution. This is in agreement with the study of Beguin et al [82] who has recently demonstrated, for double layer carbon capacitor, that hydrogen may be stored in strongly (Na_2SO_4) and weakly bonded state (KOH), depending on the nature of the electrolyte. The potential of oxidation peak of nascent hydrogen, which occurs as a consequence of deep negative polarizations, approximately corresponds to the potential of pseudo–faradaic processes, with a small shifting towards more negative values in KOH, or towards more positive values in Na_2SO_4 solution. This indicates that microporous sites, with attached oxygen atoms, are responsible for hydrogen adsorption.

The more pronounced hydrogen storage in micropores of ZTC in alkaline and neutral solution, relative to the one in acidic solution, can be clearly seen in Fig. 6, where the discharge capacitance of ZTC, obtained from anodic part of cyclic voltammograms, is presented (Fig. 5). The increase of discharge capacitance with shifting the potential towards more negative values was observed in Na_2SO_4 and particularly in KOH, while the corresponding decrease of capacitance was measured in H_2SO_4.

In all CVs given in Fig. 5, the current registered in anodic scan between the lowest negative cut–off potential and onset potential of hydrogen evolution, shows strong negative

value, indicating domination of pseudocapacitive hydrogen current over the double layer charging one. Domination of current of hydrogen oxidation over the capacitive current was also confirmed by the differences in the response of anodic peaks of ZTC in Na_2SO_4 during HER reaction: the increase of nascent hydrogen oxidation peak at positive potential and the saturation of the pseudofaradaic peak height at negative potential. Discharge capacitance of ZTC at 20 mV s^{-1} decreases when the negative potential cut–off is enlarged in H_2SO_4, due to the prolonged voltage increase, which is followed by neither process of charging of double layer nor hydrogen storage.

It may be concluded that electrochemically introduced oxygen groups upon ZTC cycling may affect the hydrogen storage capacity, since the oxygen groups block the access of hydrogen atoms into micropores [86]. Their formation at ZTC surface under anodic polarization in an acid electrolyte contributes to a poor hydrogen storage in H_2SO_4 while the absence of these groups at the surface of ZTC, upon its cycling in KOH, facilitates the hydrogen storage in ZTC.

In some literature reports related to the aqueous media, it has been shown that a decrease of surface area of ZTC causes an increase of the voltage interval of electrochemical stability [45, 49]. By comparing the CVs of here studied ZTC (S_{BET} = 1075 m^2 g^{-1}) with those reported in the literature [45, 49], in an acidic solution of common composition, it can be seen that the here studied ZTC provides higher potential window of electrochemical stability. Namely, the trend of specific surface area (S_{BET}) changing from 3689 m^2 g^{-1} [49] over 1680 m^2 g^{-1} [45] to 1075 m^2 g^{-1} [this work], is accompanied by the increasing trend of voltage window of stability in the order 0.8 V, 1.2 V and 1.4 V, respectively. Furthermore, hydrogen evolution on the surface of here studied ZTC in neutral and acidic solution was shifted much more cathodically relative to the theoretically expected potential value. The reason of this shift could be the introduction of oxygen surface groups at positive potentials, which can further block the active surface sites for electrolyte decomposition. Therefore, the material with a less developed surface area, which can be additionally deactivated by electrochemically introduced oxygen groups, may be characterized as desirable in achieving high operating voltage window.

3. 2. 3. Chronopotentiometry

Considering the values of capacitance measured by CVs, one may conclude that ZTC may be applied as an electrochemical capacitor in neutral and acidic electrolyte. Therefore,

capacitance measurements of ZTC were performed by chronopotentiometry in these two electrolytes. Galvanostatic curves of ZTC, measured in 0.5 mol dm^{-3} Na_2SO_4 and 0.5 mol dm^{-3} M H_2SO_4 at various current densities, are shown in Fig. 7. Charge capacitance (cathodic direction) amounted to 162 F g^{-1} (1 A g^{-1}), 129 F g^{-1} (2 A g^{-1}), 98 F g^{-1} (5 A g^{-1}) and 69 F g^{-1} (10 A g^{-1}) for Na_2SO_4 and 153 F g^{-1} (1 A g^{-1}), 138 F g^{-1} (2 A g^{-1}), 104 (5 A g^{-1}) and 66.5 F g^{-1} (10 A g^{-1}) for H_2SO_4 while discharge capacitance (anodic direction) amounted to 123 F g^{-1} (1 A g^{-1}), 116 F g^{-1} (2 A g^{-1}), 104 F g^{-1} (5 A g^{-1}) and 91 F g^{-1} (10 A g^{-1}) for Na_2SO_4 and 152.5 F g^{-1} (1 A g^{-1}), 140 F g^{-1} (2 A g^{-1}), 121 F g^{-1} (5 A g^{-1}) and 108.5 F g^{-1} (10 A g^{-1}) for H_2SO_4.

Although the discharge capacitance of ZTC in Na_2SO_4 is little lower than one in H_2SO_4, the use of neutral–pH aqueous electrolyte would be a more promising choice from commercial point of view. Firstly, the energy of supercapacitors is proportional to the square of the operating voltage. Therefore, the lower capacitance of ZTC in Na_2SO_4 than in H_2SO_4 is compensated by broader available voltage limit caused by water electrolysis. Second, the use of neutral solution for handling the capacitor is more friendly and easier than the use of more corrosive acidic solution.

Additionally, according to the CV and galvanostatic measurements in Na_2SO_4, ZTC has been recognized as a promising anode material for sodium aqueous rechargeable batteries.

Through a short literature survey, the above outlined capacitance values are compared to the corresponding literature values for various carbonaceous materials in aqueous solutions of sodium salts.

The capacitance of carbons in Na_2SO_4 solutions mainly arises from the electric double layer [87, 88]. Namely, the redox processes of carbonaceous materials, which are clearly evidenced in the acidic electrolyte, were found to be inactive in Na–containing aqueous solution. Hu et al. [88] demonstrated that pistachio shell–derived carbons, activated with KOH+CO_2, deliver the higher capacitance in H_2SO_4 than in aqueous electrolytes of sodium salts (Na_2SO_4 or $NaNO_3$) due to the absence of redox transition of electroactive surface functional groups in neutral media. The highest measured capacitance of these activated carbons was 112 F g^{-1} in H_2SO_4 and 80 F g^{-1} in $NaNO_3$ at 25 mV s^{-1} with the capacitance loss of 69 % for acidic electrolyte and 61 % for neutral electrolyte when the scan rate was increased up to 300 mV s^{-1}. Konno et al. [87] found that B/C/N composite, synthesized by carbonization of a mixture of polyacrylamide and boric acid, delivered very high capacitance of 300 F g^{-1} at 2 mV s^{-1} in 1 mol

dm^{-3} H_2SO_4 which originates from redox reactions of C(=O)OH group. They also measured significantly lower capacitance values in 1 mol dm^{-3} Na_2SO_4 (~ 130 F g^{-1} at 2 mV s^{-1}) due to inactivity of these processes in neutral medium. Double layer capacitance of AC in 0.5 mol dm^{-3} Na_2SO_4, without noticeable redox peaks, was also shown by Qu et al [89] who obtained the specific capacitance of ~90 F g^{-1} and ~55 F g^{-1} at 20 mV s^{-1} and 100 mV s^{-1}, respectively. Subramanian et al [90] reported double layer capacitance of carbons prepared from banana fibers treated with $ZnCl_2$ in 1 mol dm^{-3} Na_2SO_4 estimating the specific capacitance as high as 74 F g^{-1} at 500 mA g^{-1}. Double layer specific capacitance of hierarchically porous carbons (HPCs) in 2 mol dm^{-3} Na_2SO_4 [57] was amounted to 45 F g^{-1} at 1 mV s^{-1} or 33 at 1 A g^{-1}.

Béguin and coauthors [54, 91] have demonstrated the high stability potential window, (even up to 2.4 V), for carbon in Na_2SO_4 aqueous electrolyte by means of cyclic voltammetry. It opened the door for development a new generation of environmental friendly carbon/carbon capacitors. However, as showed by these authors, the operating voltage is little lower in the real two electrode arrangement. Namely, the AC/AC symmetric capacitor [91] in 0.5 mol dm^{-3} Na_2SO_4 could operate up to 1.6 V with a specific capacitance of 135 F g^{-1}. Wang et al. [92] assembled symmetric capacitor, composed from three–dimensional flower like and hierarchical porous carbon material (FHPC), with 1mol dm^{-3} Na_2SO_4 as aqueous electrolyte which operated in the voltage range from 0 to 1.8 V with maximal high energy density of 15.9 Wh kg^{-1} and a power density of 317.5 W kg^{-1}. The charge storage of FHPC in Na_2SO_4 was found to arise from double layer capacitance.

Fic et al [55] have demonstrated the operating voltage of real two–electrode capacitor as high as 2.2 V by using the Li_2SO_4 as aqueous electrolytic solution. They measured better capacitance of carbon in Li_2SO_4 (170 F g^{-1}) then in Na_2SO_4 (105 F g^{-1}), especially at high current rates.

Apart from high voltage, Beguin's groups [54] reported the pseudofaradaic reactions of seaweed carbon in neutral electrolyte as was also demonstrated for the ZTC material. Thanks to the pseudocapacitance behavior in Na_2SO_4, these authors reported the specific capacitance of 121 F g^{-1} (600 ^oC) and 115 F g^{-1} (750 ^oC) with a very high stability potential window up to 2.4 V. However, the real symmetric capacitor composed from these seaweed carbons could operate up to 1.6 V in Na_2SO_4. It was shown that carbon with a higher capacitance showed lower specific surface area and higher amount of all functional groups particularly quinone groups.

The measured capacitance values of ZTC in Na_2SO_4 fall within the range of those (from 70 to 130 F g^{-1}) reported for different carbonaceous materials in neutral electrolytes. Due to the less developed surface area, the specific capacitance in both acidic and neutral electrolytes was significantly lower than the ones measured for highly ordered ZTCs in acidic [45, 47, 49] and alkaline solution [46]. However, in Na_2SO_4 solution, almost twice as much voltage window of stability was found as that provided by highly ordered ZTCs [45-47, 49]. Therefore, from the aspect of capacitor energy density, the here examined material could be comparable to the other ZTCs. Also, in addition to a simpler and shorter synthesis of here studied ZTC, Na_2SO_4 as a neutral electrolyte, is environmentally more friendly than either acidic or alkaline solution. Furthermore, confirmation of carbon faradaic reactions in neutral medium opens new directions in regard of increasing the capacitance of "neutral" carbon capacitors through the improvement of activity of redox processes.

3.2.4. Impedance analysis

In order to get deeper understanding of complex pseudo–capacitance processes at the ZTC/electrolyte interface, impedance measurements and the complex capacitance analysis, were performed. Since double layer and charge transfer based charge storage have different time constants, and consequently display impedance response at different frequency intervals, the impedance measurement within wide frequency range is a very useful tool for their separate analysis.

The Nyquist plots of ZTC in 6 mol dm^{-3} KOH, 0.5 mol dm^{-3} Na_2SO_4 and 0.5 mol dm^{-3} H_2SO_4, measured within common frequency range from 0.01Hz to 10^6 Hz at different polarization potentials, are presented in Fig. 8a. The sum consisted of ohmic electrolyte resistance and internal resistance of electrode material, marked as R_s, is determined as a high frequency intercept on the real axis in Nyquist plots, and amounted to ~ 2.6 Ω, 3.1 Ω and 5.2 Ω in KOH, H_2SO_4 and Na_2SO_4, respectively. These values are controlled by the molar conductivity of all electrolyte ions (the best is for highly mobile OH^- and H^+ ions) [57].

Three characteristic parts in the Nyquist diagrams of ZTC were observed: depressed semicircle at high frequency which indicates the fast pseudofaradaic processes, small diffusion limited porous region with slope ~ 45º slope and a linear part in the region of the low frequencies. Generally, the vertical line of the Nyquist plot in the low frequency region as well as the value of

phase angle close to 90º, indicates an ideal capacitance behavior. Deviation of the low frequency Nyqist plot from the vertical line (Fig. 8a) or deviation of phase angle from the 90º value (Fig. 8b) can be attributed to the interaction of the carbon surface with the ions, depending on the applied potential, as also confirmed by CVs.

The impedance behavior of ZTC was further studied using the complex capacitance model [93] according to the equations presented in Supp. Information.

Fig. 8c and Fig. 8d show the dependence of real part of the capacitance ($C'(\omega)$) and imaginary part of capacitance ($C''(\omega)$) with frequency for ZTC, in all aqueous electrolytes. $C'(\omega)$ and $C''(\omega)$ increase when the frequency is decreased, in dependence of used aqueous electrolyte and polarization potential.

The dependence of $C'(\omega)$ on frequency for all capacitors can generally be described as follows: $C'(\omega)$ sharply increases as the frequency decreases, where is in the low frequency region $C'(\omega)$ tends to become frequency independent due to whole accessibility of pores to electrolyte ions [93–95]. The absence of such low–frequency behavior of $C'(\omega)$ for ZTC indicates that material is not fully accessible at 0.01 Hz because the ions, in spite of low frequencies, may not still penetrated into all micropores. The reason for that could be the existence of ultramicropores in ZTC which are less from 0.7 nm [83, 96] and which can be also responsible for the strong hydrogen storage in ZTC in alkaline and neutral solution. The value of capacitance, determined at the lowest frequency (C_{LF}), at the potentials where the redox activity is the most pronounced (–0.7 V vs. SCE for KOH, –0.4 V. vs. SCE for Na_2SO_4 and 0.6 V vs. SCE for H_2SO_4), follows the capacitance trend measured by both cyclic voltammetry and constant current measurements. The similar C_{LF} values of ZTC in KOH and Na_2SO_4 was obtained at common negative potential of –0.7 V vs. SCE, which is also in agreement with the cyclic voltammetric measurements. The sharper increase of $C'(\omega)$ curves in Na_2SO_4 (–0.4 V vs. SCE) and H_2SO_4 (0.4 V vs. SCE) than in KOH is due to more pronounced pseudofaradaic reactions at these potentials.

Regarding the dependence of $C''(\omega)$ versus frequency, the common behavior of carbon capacitors is that the $C''(\omega)$ curve passes through the maximum. The frequency value (f_o) at the $C''(\omega)$ maximum corresponds to the relaxation time constant τ_o. This is point where the system changes behavior from resistor to capacitor and is generally regarded as a quantitative measure of the rate capability. Namely, τ_o as characteristic of the whole system is defined as $1/f_o$ and its lower value (higher f_o) generally indicates the higher power density (faster delivery of stored

energy). Although the maximum of the $C''(\omega)$ curves in both KOH and Na_2SO_4 solutions is not well defined, the relaxation time constant, expressed as $\tau_o=1/f_{o,}$ can be estimated to be 6.25 s (–0.7 V) for KOH, 10 s (–0.4 V) or 13.7 s (–0.7 V) for Na_2SO_4 and 31 s (0.4 V) for H_2SO_4. The lower value of τ_o measured for ZTC in KOH compared to the ones in Na_2SO_4 and H_2SO_4 solutions, indicates a faster charging/discharging of ZTC, in spite of its the lowest capacity in KOH. One can conclude that the trend of the time constant increase follows the trend of the pseudocapacitance increase. Namely, the increase of the capacitance, due to more pronounced redox reactions, results in the higher relaxation time constant i.e. longer time needed to achieve complete capacity.

In summary, the results of cyclic voltammety and impedance measurements show that the charge storage mechanism of ZTC, in different aqueous electrolytes, originates from both double–layer capacitance and pseudocapacitance. Their relative contribution can vary, depending on the type of electrolyte which controls the degree of pseudofaradaic reactions activity. Double layer capacitance plays the dominant role in the charging of ZTC in KOH while the pseudocapacitance, expressed through quinone reactions, is dominant in H_2SO_4. It was shown that the capacitance behavior of ZTC in neutral Na_2SO_4 solution was balanced between behavior in both acid and alkaline solutions. Actually, the capacitance of ZTC follows trend H_2SO_4>Na_2SO_4>KOH while its drop with scan rates follows the opposite trend. Therefore, the use of Na_2SO_4 as an aqueous electrolyte for operating the ZTC as capacitor can be regarded as an optimum choice. Furthermore, the highest stability potential window of ZTC in the Na_2SO_4 made this neutral electrolyte the most perspective for constructing the ZTC aqueous–type capacitor.

4. Conclusions

A highly microporous zeolite-templated carbon (ZTC) was prepared using zeolite Y (Na–form) as a template and furfuryl alcohol as a carbon precursor. Structural characterization of the carbon powder indicates that the complete structure regularity of the template has not been achieved by simple impregnation method, which is known obstacle of zeolite templating procedure. Namely, ZTC has a quite high volume of micropores but also a certain fraction of the mesopores. The pseudocapacitance behavior of ZTC was found to be typical for each aqueous solution even for the neutral one. It was shown that pseudo–faradaic contribution, specific capacitance, hydrogen storage capacity, strength H–C bond and relaxation time constant of ZTC

are affected by the type of electrolytic solution. The decrease in electrolyte pH makes the oxygen groups at the surface more active, resulting in an increase in ZTC capacitance. The capacitance loss at a high scan rate of 100 mV s^{-1} follows the same trend: KOH < Na_2SO_4 < H_2SO_4. This was explained by the differences in the redistribution of the charge in the "inner" and "outer" part of carbon surface versus scan rate in different aqueous electrolytes. Furthermore, besides the porous carbon texture, the oxygen surface groups, created at positive potentials under anodic polarization, are another important factor in the effective utilization of ZTC surface for hydrogen storage as well as in the voltage limits setting. Finally, thanks to both high stability potential window (2.3 V at 20 mV s^{-1}) and relatively high capacitance utilization of this material (123 F g^{-1} at 1 A g^{-1}) in an aqueous Na_2SO_4 solution, neutral electrolyte was found to be more promising electrolyte for the ZTC capacitor, being cost–effective, non–corrosive and environment–friendly and enabling broadest voltage window limited by water electrolysis.

Acknowledgement

This work was supported by the Serbian Ministry of Education, Science, and Technological Development through the projects III 45012 and III 45014. MV and SM are indebted for financial support by NATO through the Science for Peace Project EAP.SFPP 984925–DURAPEM. The authors are thankful to prof. Zlatko Rakočević, Dr. Nenad Bundaleski and Dr. Maja Popović from the Laboratory of Atomic Physics of the Vinča Institute of Nuclear Science, University in Belgrade, for performing XPS analysis and helping in its interpretation.

5. References

[1] J. Chmiola, G. Yushin, Y. Gogotsi, C. Portet, P. Simon, P.L. Taberna, *Science* 313 (2006) 1760–1763.

[2] J. Chmiola, C. Largeot, P.L. Taberna, P. Simon, Y. Gogotsi, Angew. Chem. Int. Ed. 47 (2008) 3392–3395.

[3] D. Hulicova–Jurcakova, M. Seredych, G.Q. Lu, T.J. Bandosz, Adv. Funct. Mater. 19 (2009) 438–447.

[4] X. Zhang, M. Wu, M. Zheng, J. Phys. Chem. Solid. 70 (2009) 738–744.

[5] X. Xia, L. Shi, H. Liu, L. Yang, Y. He, J. Phys. Chem. Solid. 73 (2012) 385–390.

[6] M. Seredych, D. Hulicova–Jurcakova, G.Q. Lu, T.J. Bandosz, Carbon, 46 (2008) 1475–1488.

[7] C. Moreno–Castilla, M.B. Dawidzuik, F. Carrasco–Marin, E. Morallón, Carbon 50 (2012) 3324–3332.

[8] N. Gavrilov, I. Pašti, M. Vujković, G. Ćirić–Marjanović, J. Travas–Sejdić, S. Mentus, Carbon 50 (2012) 3915–3927.

[9] M. Vujković, N. Gavrilov, I. Pašti, J. Krstić, J. Travas–Sejdić, G. Ćirić–Marjanović, S. Mentus, Carbon 64 (2013) 472–486.

[10] C. Largeot, C. Portet, J. Chmiola, P.L. Taberna, Y. Gogotsi, P. Simon, J. Am. Chem. Soc. 130 (2008) 2730–2731.

[11] C. Hsieh, H. Teng, Carbon 40 (2002) 667–674.

[12] M. Inagaki, H. Konno, O. Tanaike, J. Power Sources 195 (2010) 7880–7903.

[13] M.J. Bleda–Martínez, D. Lozano–Castello, E. Morallón, D. Cazorla–Amaros, A. Linares–Solano, Carbon 44 (2006) 2642–2651.

[14] P. Simon, Y Gogotsi, Phil. Trans. R. Soc. A 368 (2010) 3457–3467.

[15] K. Fic, E. Frackowiak, F. Béguin, J. Mater. Chem. 22 (2012) 24213–24223.

[16] C. Moreno–Castilla, M.A. Ferro–Garcia, J.P. Joly, I. Bautista–Toledo, F. Carrasco–Marin, J. Rivera–Utrilla, Langmuir 11 (1995) 4386–4392.

[17] J. Zhang, H. Zou, Q. Qing, Y. Yang, Q. Li, Z. Liu, X. Guo, Z. Du, J. Phys. Chem. B 107 (2003) 3712–3718.

[18] P.A. Bazuła, A.H. Lu, J.J. Nitz, F. Schuth, Microp. Mesop. Mater. 108 (2008) 266–275.

[19] P. Solís–Fernández, J.I. Paredes, S. Villar–Rodil, L. Guardia, M.J. Fernández–Merino, G. Dobrik, L.P. Bíro, A. Martinez–Alonso, J.M.D. Tascón, J Phys. Chem. C 115 (2011) 7956–7966.

[20] E.C. Landis, K.L. Klein, A. Liao, E. Pop, D.K. Hensley, A.V. Melechko, R.J. Hamers, Chem. Mater. 22 (2010) 2357–2366.

[21] T. Kyotani, Bull. Chem. Soc. Jpn. 79 (2006) 1322–1337.

[22] T. Kyotani, Carbon 38 (2000) 269–286.

[23] C. Liang, Z. Li, S. Dai, Angew Chem. Int. Ed. 47 (2008) 3696–3717.

[24] J. Lee, S. Han, T. Hyeon, J Mater. Chem. 14 (2004) 478–486.

[25] A. H. Lu, F. Schuth, Adv. Mater. 18 (2006) 1793–1805.

[26] H. Yang, D. Zhao, J. Mater. Chem. 15 (2005) 1217–1231.

[27] Y. Xia, Z. Yang, R. Mokaya, Nanoscale 2 (2010) 639–659.

[28] E.C. Landis, K.L. Klein, A. Liao, E. Pop, D.K. Hensley, A.V. Melechko, R.J. Hamers, Chem. Mater. 22 (2010) 2357–2366.

[29] T. Kyotani, T. Nagai, A. Tomita, Extended Abstracts of Carbon 92 (1992) 437–439.

[30] H. Nishihara, T. Kyotani, Zeolite–Templated Carbon–Its Unique Characteristics and Applications, in: J. M. D. Tascón, Novel Carbon Adsorbents, Elsevier Ltd. pp. 295–322.

[31] T. Kyotani, T. Nagai, S. Inoue, A. Tomita, Chem. Mater. 9 (1997) 609–615.

[32] J. Rodriguez–Mirasol, T. Cordero, L.R. Radovic, J.J. Rodriguez, Chem. Mater. 10 (1998) 550–558.

[33] S.A. Johnson, E.S. Brigham, P.J. Ollivier, T.E. Mallouk, Chem. Mater. 9 (1997) 2448–2458.

[34] C.J. Meyers, S.D. Shah, S.C. Patel, R.M. Sneeringer, C.A. Bessel, N.R. Dollahon, R.A. Leising, E.S. Takeuchi, J. Phys. Chem. B. 105 (2001) 2143–2152.

[35] Z. Ma, T. Kyotani, A. Tomita, Chem. Commun. (2000) 2365–2366.

[36] Z. Ma, T. Kyotani, A. Tomita, Carbon 40 (2002) 2367–2374.

[37] Y. Kojima, H. Miyaoka, T. Ichikawa, Hydrogen Storage Materials, in Steven L. Suib. (Ed.), New and Future Developments in Catalysis: Batteries, Hydrogen Storage and Fuel Cells, Elsevier, 2013, Ch. 5, pp.131.

[38] T. Kyotani, Z. X. Ma, A. Tomita, Carbon 41 (2003) 1451–1459.

[39] F.B. Su, H.J. Zeng, Y.J. Yu, L. Lv, J.Y. Lee, X.S. Zhao, Carbon 43 (2005) 2368–2373.

[40] Z.X. Yang, Y.D. Xia, R. Mokaya, J.Am. Chem. Soc. 129 (2007) 1673–1679.

[41] F.O. M. Gaslain, J. Parmentier, V.P. Valtchev, J. Patarin, Chem. Commmun. (2006) 991–993.

[42] E. Frackowiak, Phys. Chem. Chem. Phys. 9 (2007) 1774–1785.

[43] J. Chmiola, G. Yushin, R.K. Dash, E.N. Hoffman, J.E. Fischer, M.W. Barsoum, Y. Gogotsi, Electrochem. Solid State Commun. 8 (2005) A357–A360.

[44] G. Yushin, E. Hoffman, A. Nikitin, H. Ye, M.W. Barsoum, Y. Gogotsi, Carbon 44 (2005) 2075–2082.

[45] C.O. Ania, V. Khomenko, E. Raymundo–Pinero, J.B. Parra, F. Beguin, Adv. Funct. Mater. 17 (2007) 1828–1836.

[46] H. Wang, Q. Gao, J. Hu, Microporous Mesoporous Mater. 131 (2010) 89–96.

[47] A. Kajdos, A. Kvit, F. Jones, J. Jagiello, G. Yushin, J. Am. Chem. Soc. 132 (2010) 3252–3253.

[48] Y. Korenblit, A. Kajdos, W.C.West, M.C. Smart, E.J. Brandon, A. Kvit, J. Jagiello, G. Yushin, Adv. Funct. Mater. 22 (2012) 1655–1662.

[49] H. Itoi, H. Nishihara, T. Ishii, K. Huaengnoraj, R. Berenguer-Betrián, T. Kyotani, Bull. Chem. Soc. Jpn. 87 (2014) 250-257.

[50] C. Portet, Y. Korenblit, Y Gogotsi, R Mokaya, G. Yushin, J. Electrochem. Soc. 156 (2009) A1–A6.

[51] H. Itoi, H. Nishihara, T Kogure, T. Kyotani, J. Am. Chem. Soc. 133 (2011) 1165-1167.

[52] R. Berengure, H. Nishihara, H. Itoi, T. Ishii, E. Morallón, D. Cazorla–Amorós, T. Kyotani, Carbon 54 (2013) 94–104.

[53] A. Burke, Electrochim. Acta. 53 (2007) 1083–1091.

[54] M.P. Bichat, E. Raymundo–Piñero, F. Béguin, Carbon 48 (2010) 4351–4361.

[55] K. Fic, G. Lota, M. Meller, E. Frackowiak, Energy Environ. Sci. **5** (2012) 5842–5850.

[56] Q. Gao, L. Demarconnay, E. Raymundo–Piñero, F. Béguin, Energy Environ. Sci. **5** (2012) 9611–9617.

[57] X. Zhang, X. Wang, L. Jiang, H. Wu, C. Wu, J. Su, J. Power Sources 216 (2012) 290–296.

[58] H.A. Andreas, B.E. Conway, Electrochim. Acta 51 (2006) 6510–6520.

[59] F. Rouquerol, J. Rouquerol and K. S. W. Sing, Adsorption by Powders and Porous Solids, Academic Press, London, 1998.

[60] M. M. Dubinin, In: Cadenhead D.A., editor. Progress in Surface and Membrane Science, 9. New York: Academic Press, 1975, pp. 1–70.

[61] G. Horvath, K. Kawazoe, J. Chem. Eng. Jpn. 16 (1983) 470–475.

[62] S.J. Gregg, K.S.W. Sing, 41. London: Academic Press; 1982, pp. 195.

[63] M. Kruk, M. Jaroniec, P. K. P. Gadkaree, Journal of Colloid and Interface Science, 1997, 192, pp. 250–256.8

[64] A. Lecloux, J.P. Pirard, J. Colloid Interf. Sci. 70 (1979) 265–281.

[65] K.S.W. Sing, D.H. Everett, R.A. W Haul, L. Moscou, R.A. Pierotti, J. Rouquérol, T. Siemieniewska, Pure Appl. Chem. 57 (1985) 603–619.

[66] A. Pacula, R. Mokaya, J. Phys. Chem. C 112 (2008) 2764–2769.

[67] N. Alam, R. Mokaya, Energy Environ. Sci. 3 (2010) 1773–1781.

[68] A.M. Silvestre–Albero, J.M. Juárez–Galán, J. Silvestre–Albero, F. Rodríguez–Reinoso, J. Phys. Chem. C 116 (2012) 16652–16655.

[69] C. Reichenbach, D. Enke, J. Möllmer, D. Klank, M. Klauck, G. Kalies, Micropor. Mesopor. Mater. 181 (2013) 68–73.

[70] S.A Johnson, E.S. Brigham, P.J. Ollivier, T.E. Mallouk, Chem. Mater. 9 (1997) 2448–2458.

[71] Y.Z. Jin, C. Gao, W.K. Hsu, Y.Q. Zhu, A. Huczko, M. Bystrzejewski, M. Roe, C.Y. Lee, S. Acquah, H. Kroto, D.R.M. Walton, Carbon 43 (2005) 1944–1953.

[72] P.X. Hou, T. Yamazaki, H. Orikasa, T. Kyotani, Letters to the Editor/Carbon 43 (2005) 2618–2641.

[73] F. Su, X.S. Zhao, L.L.Z. Zhou, Carbon 42 (2004) 2821–2831.

[74] K. Guérin, J.P. Pinheiro, M. Dubois, Z. Fawal, F. Masin, R. Yazami, A. Hamwi, Chem. Mater. 16 (2004) 1786–1792.

[75] A.C. Ferrari, J. Robertson, Phys. Rev. B 61 (2000) 14095–14107.

[76] S. Biniak, G. Szymanski, J. Siedlewski, A. Swiatkovski, Carbon, 35 (12) 1799-1810.

[77] M.A. Montes–Morán, D. Suárez, J.A. Menéndez, E. Fuente, Carbon 42 (2004) 1219–1225.

[78] V. Khomenko, E. Raymundo–Piñero, A. Béguin, J Power Sources 195 (2010) 4234–4241.

[79] Y. Tian, R. Xue, X. Zhou, Z. Lium, L. Huang, Electrochim. Acta 152 (2015) 135–139.

[80] J. Eskusson, A Jänes, A. Kikas, L. Matisen, E. Lust, J. Power Sources 196 (2011) 4109–4116.

[81] S. Ardizone, G. Fregonara, S. Trasatti, Electrochim. Acta 35 (1990) 263–267.

[82] S. Leyva–Garcia, E. Morallón, D. Cazorla–Amorós, F. Béguin, D. Lozano–Castelló, Carbon 69 (2014) 401–408.

[83] F. Béguin, K. Kierzek, M. Friebe, A. Jankowska, J. Machnikowski, K. Jurewicz, E. Frackowiak, Electrochim. Acta 51 (2006) 2161–2167.

[84] K. Jurewicz, E. Frackowiak, Appl. Phys. A 78 (2004) 981–987.

[85] K. Babel, D. Janasiak, K. Jurewicz, Carbon 50 (2012) 5017–5026.

[86] M.J. Bleda–Martínez, J.M. Péres, A. Linares–Solano, E. Morallón, D. Cazorla–Amorós, Carbon 46 (2008) 1053–1059.

[87] H. Konno, T. Ito, M. Ushiro, K. Fushimi, K. Azumi, J Power Sources 195 (2010) 1739–1746.

[88] C.C. Hu, C.C. Wang, F.C. Wu, R.L. Tseng, Electrochim. Acta 52 (2007) 2498–2505.

[89] Q.T. Qu, B. Wang, L.C. Yang, Y. Shi, S. Tian, Y.P. Wu, Electrochem. Commun. 10 (2008) 1652–1655.

[90] V. Subramanian, A.M. Stephan, K.S. Nahm, S. Thomas, B. Wei, J. Phys. Chem. C 111 (2007) 7527–7531.

[91] L. Demarconnay, E. Raymundo–Piñero, F. Béguin, Electrochem. Commun. 10 (2010) 1275–1278.

[92] Q. Wang, J. Yan, Y. Wang, T. Wei, M. Zhang, X. Jing X, Z. Fan, Carbon 67 (2014) 119–127.

[93] P.L. Taberna, P. Simon, J.F. Fauvarque, J. Electrochem. Soc. 150 (2003) 292–300.

[94] J. Zhou, Z. Zhang, W. Xing, J. Yu, G. Han G, W. Si, S. Zhuo, Electrochim. Acta 153 (2015) 68–75.

[95] C. Cougnon, E. Lebègue, G. Pognon, J. Power Sources 274 (2015) 551–559.

[96] M. Rzepka, P. Lamp, M.A. de la Casa–Lillo, J. Phys. Chem. B 102 (1998) 10894–10898.

Figure captions:

Figure 1. a) N_2–physorption isotherms (●–adsorption, ○–desorption); inset gives enlarged part of their low pressure region; b) the pore size distribution curves (PSD) of the ZTC in the micropore region obtained by HK method; c) and d) SEM images of investigated ZTC sample under two different magnifications.

Figure 2. C1s (a) and O1s (b) spectra of ZTC sample and their fitting curves.

Figure 3. The cyclic voltammograms of ZTC measured at different scan rates in 6 mol dm^{-3} KOH a), 0.5 mol dm^{-3} Na_2SO_4 b) and 0.5 mol dm^{-3} H_2SO_4 c), normalized by scan rate.

Figure 4. Cyclic voltamograms of ZTC measured in different aqueous electrolytes within various potential regions. The scan rate was 20 mV s^{-1}.

Figure 5. Cyclic voltammograms (CV's) of ZTC measured in 6 mol dm^{-3} KOH (a), 0.5 mol dm^{-3} Na_2SO_4 (b) and 0.5 mol dm^{-3} H_2SO_4 (c) at a common 20 mV s^{-1} scan rate with a stepwise shift (steps of 100 mV) of negative potential cut–off. Inset shows the enlarged part of nascent oxidation peak. The vertical line corresponds to the hydrogen equilibrium potential in corresponding electrolyte at 25 ^oC.

Figure 6. Discharge capacitances obtained by integration of CV's presented in Figure 5.

Figure 7. Galvanostatic curves of ZTC measured at different current densities in 0.5 mol dm^{-3} Na_2SO_4 (a) and 0.5 mol dm^{-3} H_2SO_4 (b).

Figure 8. Impedance analysis of ZTC sample at various potentials vs. SCE, in different aqueous electrolytes: a) Nyquist plots (inset shows its magnification in high frequency region), b) phase angle vs. frequency plot, c) real part of the capacitance vs. frequency plot, and d) imaginary capacitance vs. frequency plot.

Tables:

Table 1. Textural parameters of ZTC sample

ZTC sample	
S_{BET} / m^2 g^{-1}	1075
$S\alpha_s$ / m^2 g^{-1}	509
$S_{meso-\alpha_s}$ / m^2 g^{-1}	51.4
$V_{meso-BJH}$ / cm^3 g^{-1}	0.165
$V_{mic-\alpha_s}$ / cm^3 g^{-1}	0.438
V_{mic-HK} / cm^3 g^{-1}	0.441
V_{mic-DR} / cm^3 g^{-1}	0.400

Table 2. Specific capacitance (F g^{-1}) of ZTC in the aqueous electrolytic solutions calculated from cyclic voltammograms measured at various scan rates.

Aqueous Electrolyte	***Potential sweep rate / mVs^{-1}***					
Specific capacitance Fg^{-1}	10	20	30	40	50	100
6 mol dm^{-3} KOH	80	65	62	59	57	50
	64	60	58	56	54	47
0.5 mol dm^{-3} Na_2SO_4	127	111	104	99	94	78
	104	101	97	93	89	75
0.5 mo ldm^{-3} H_2SO_4	150	131	118	110	101	82
	143	126	115	106	100	77

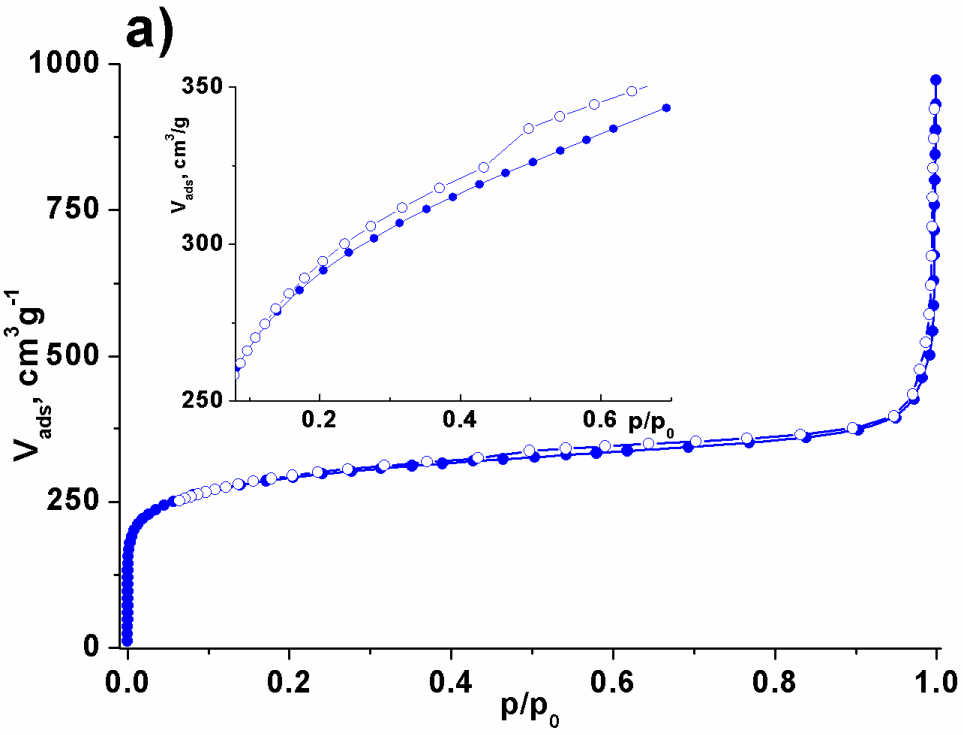

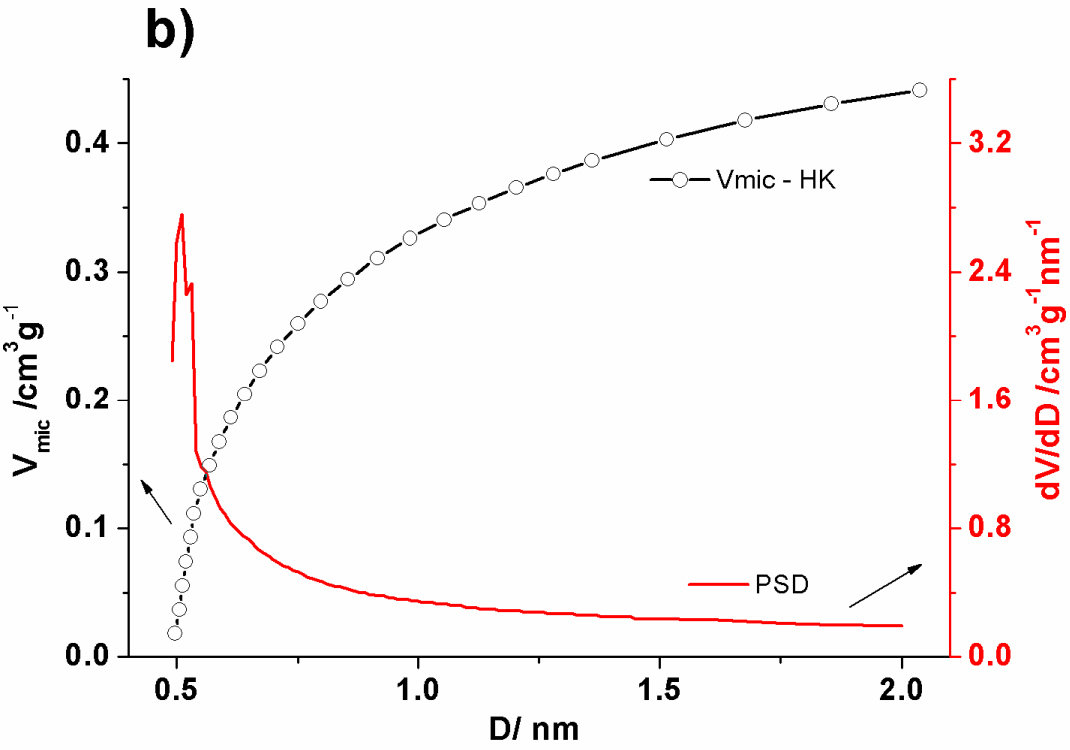

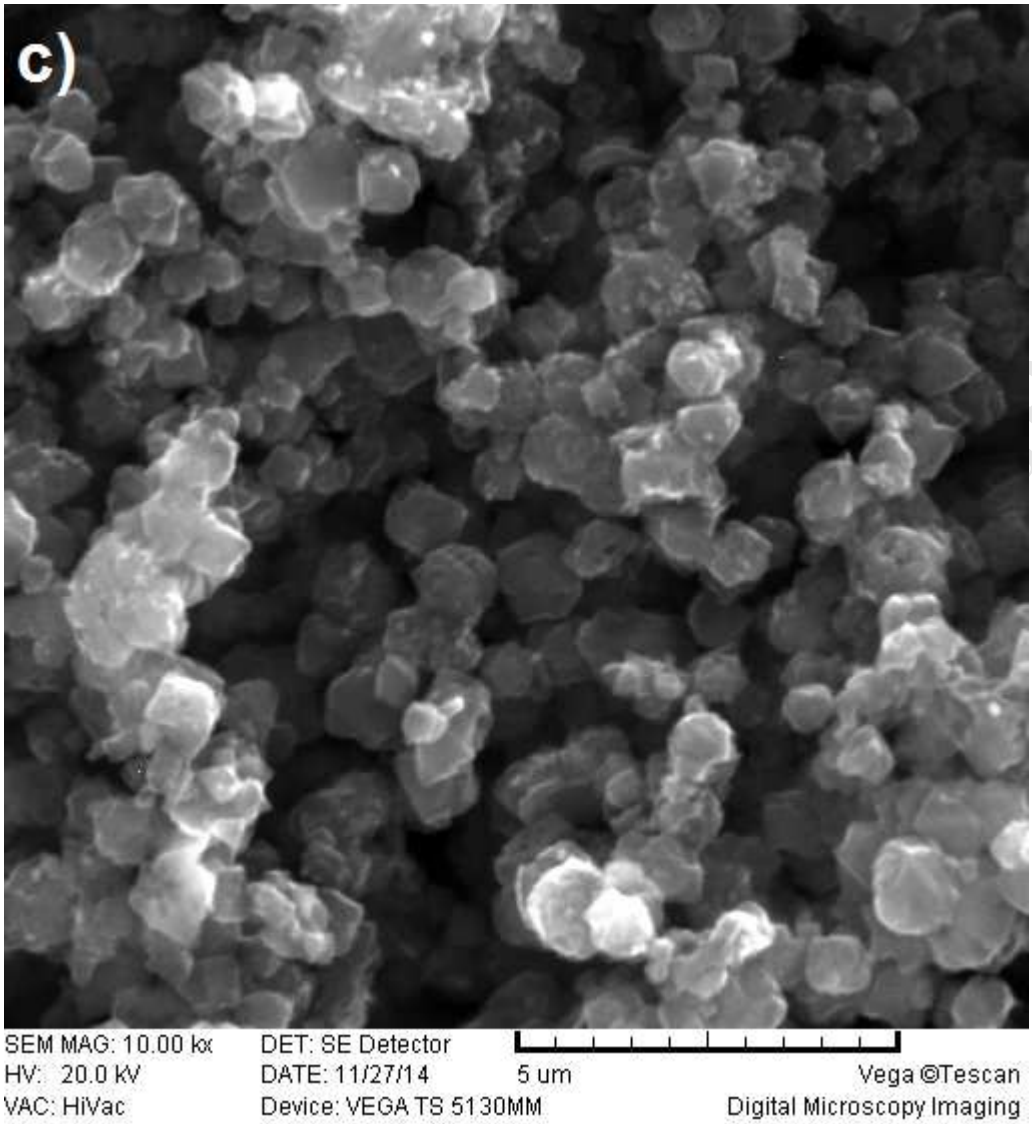

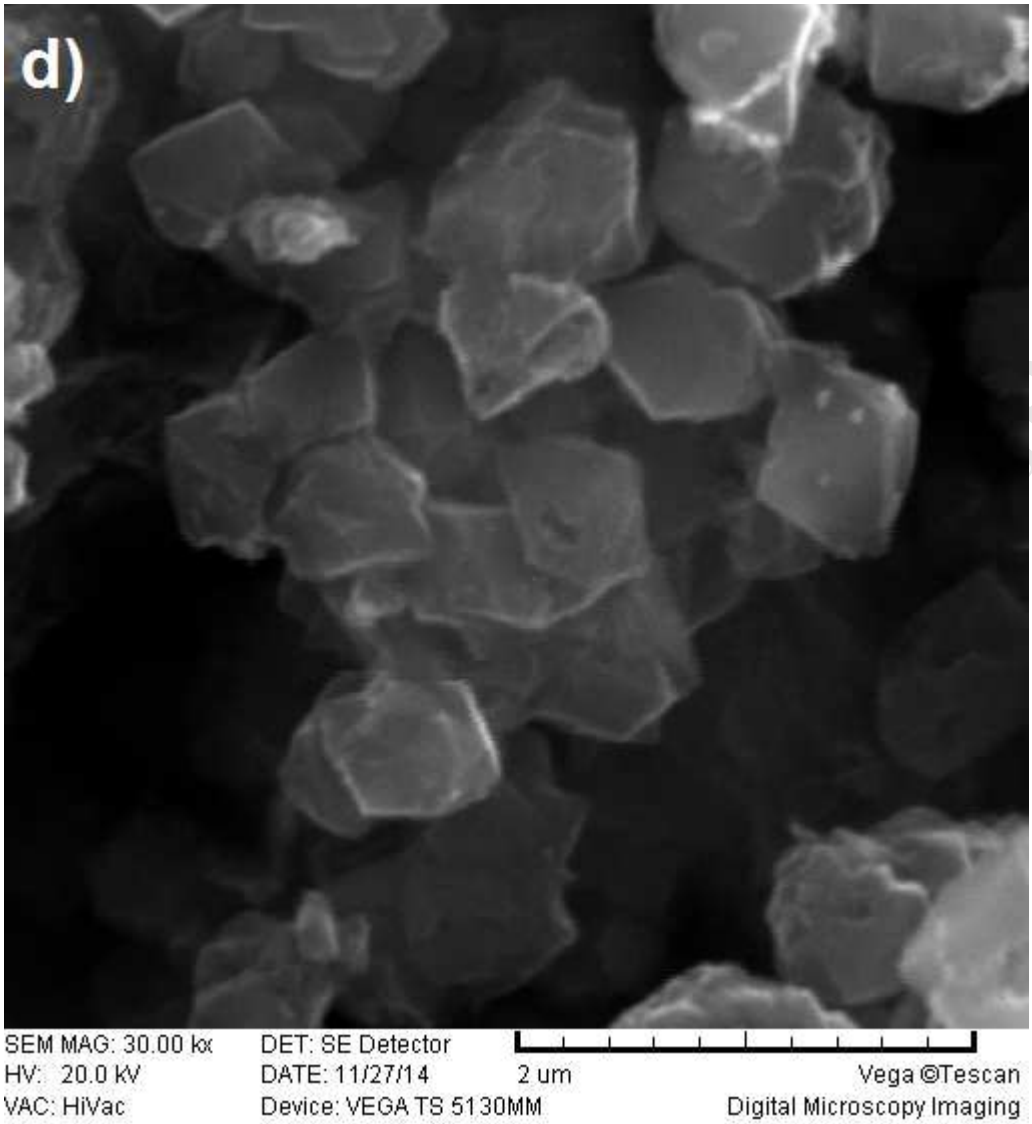

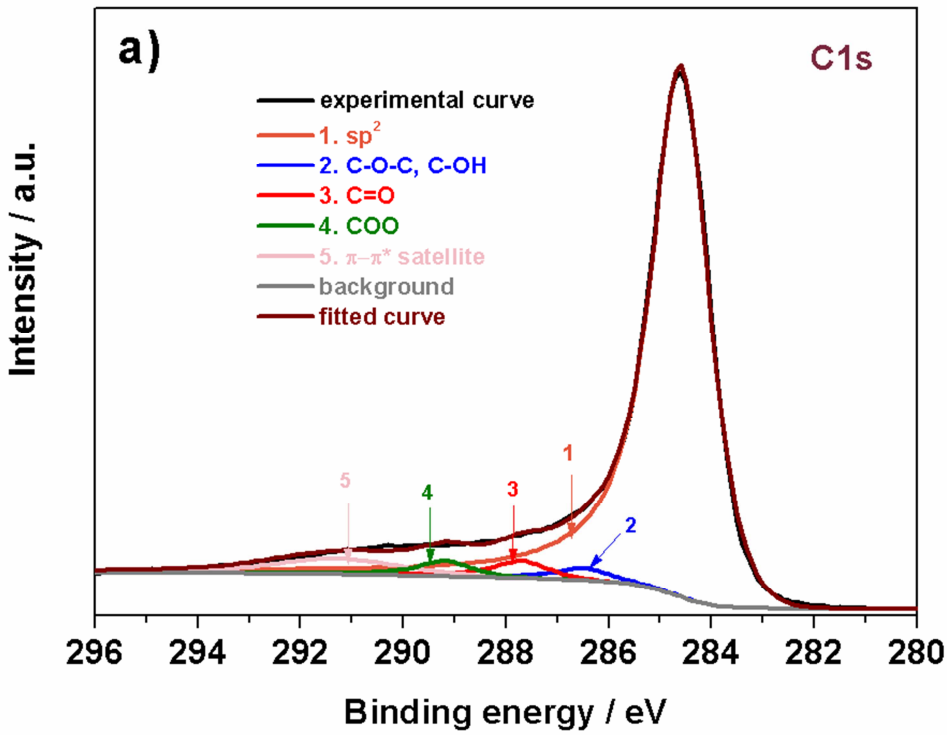

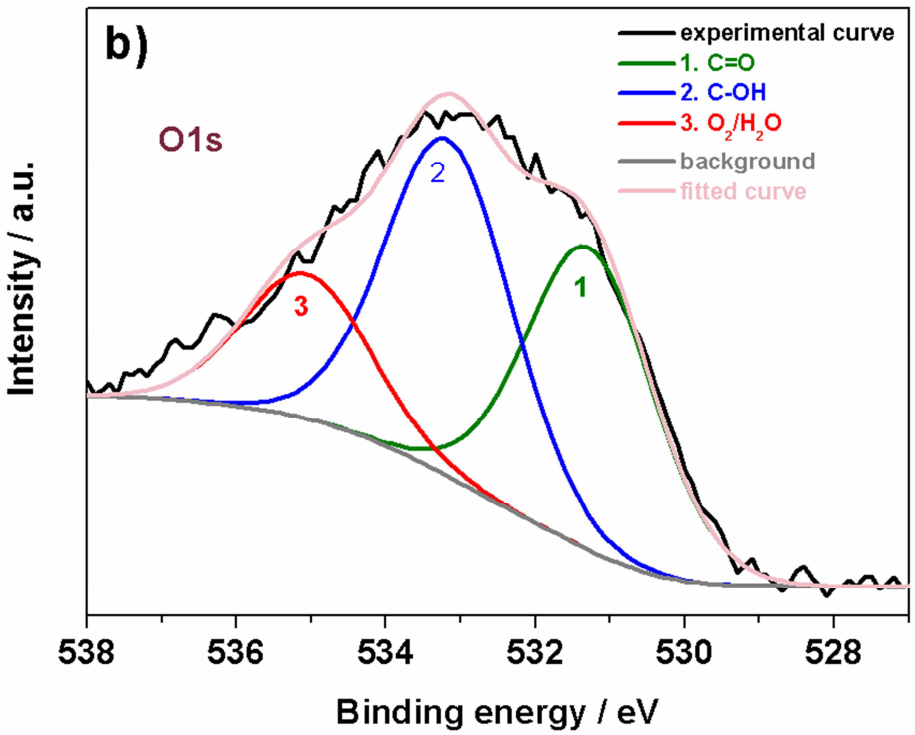

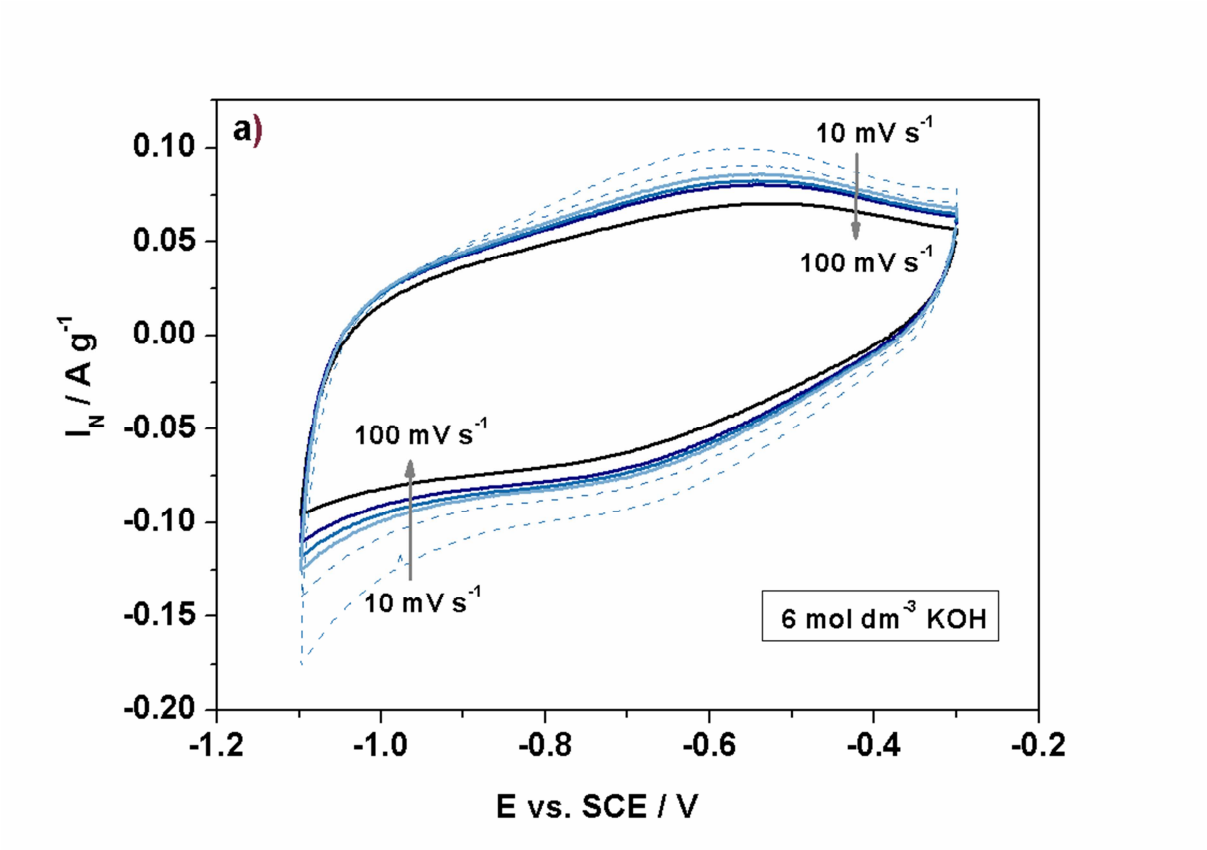

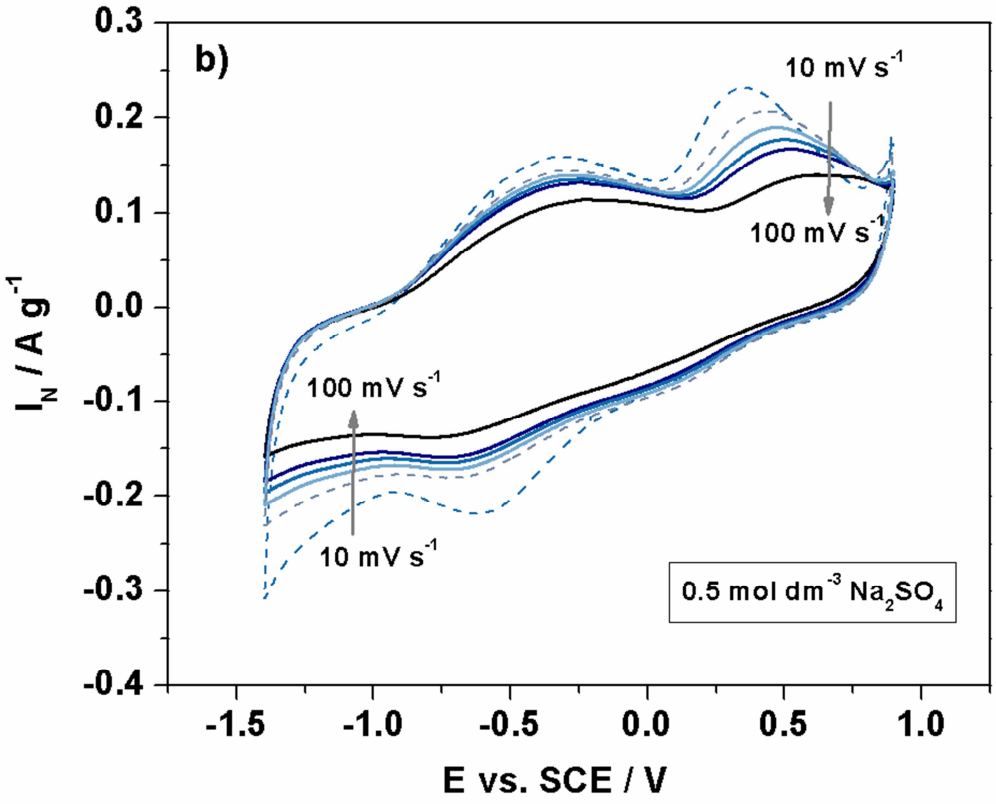

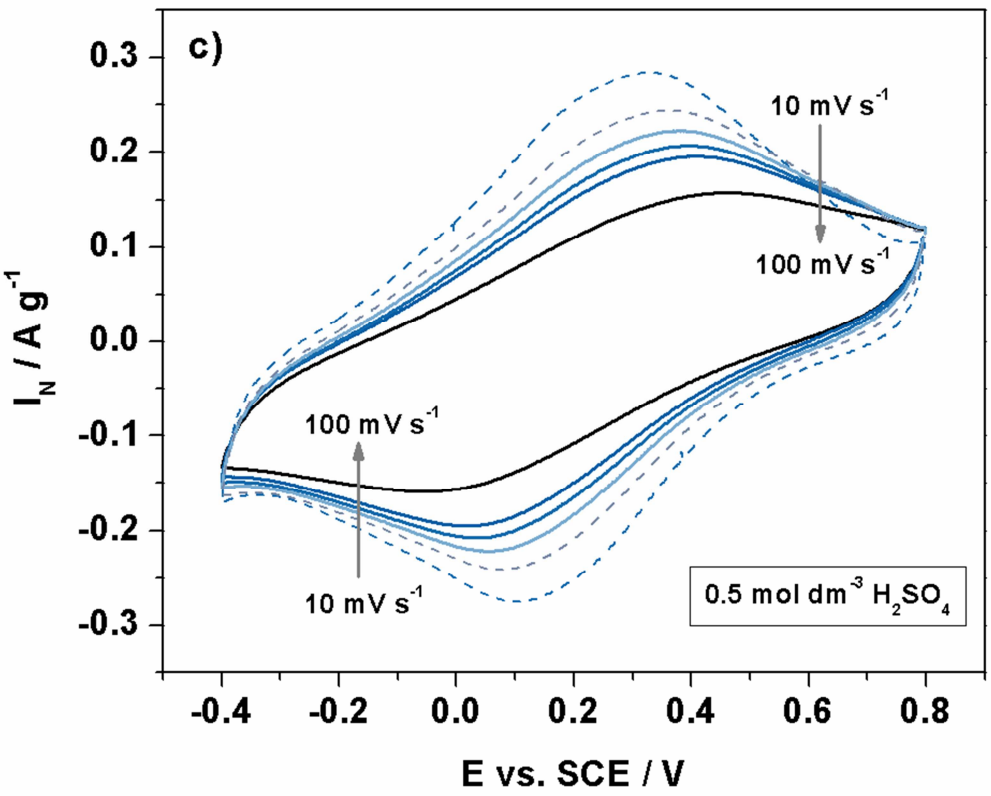

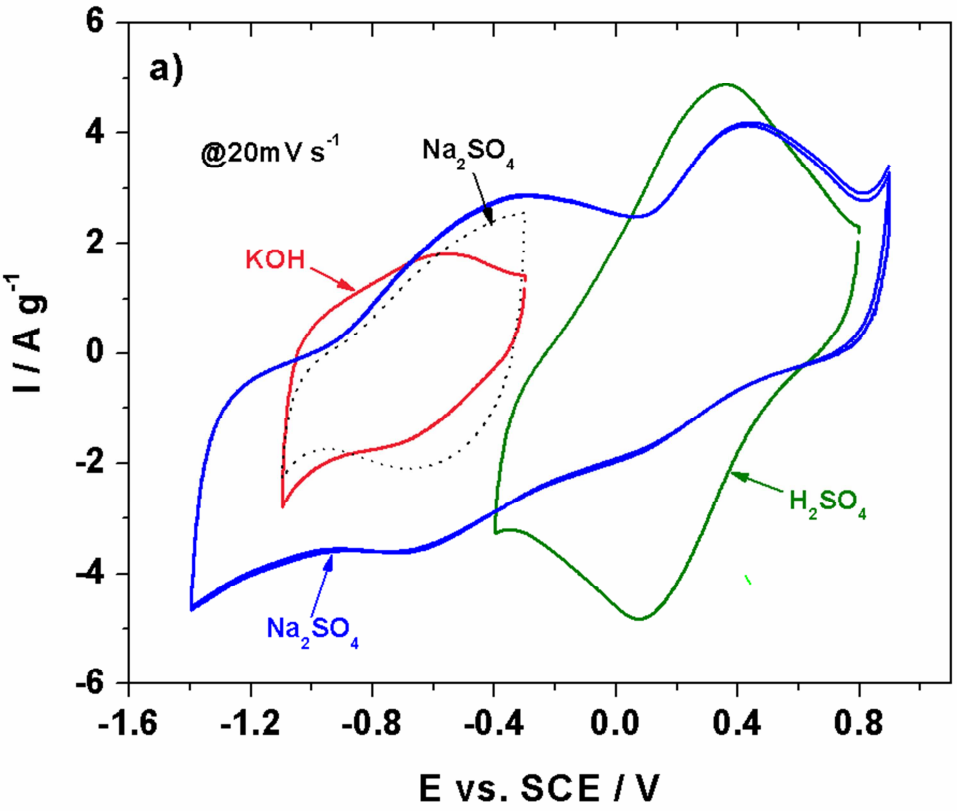

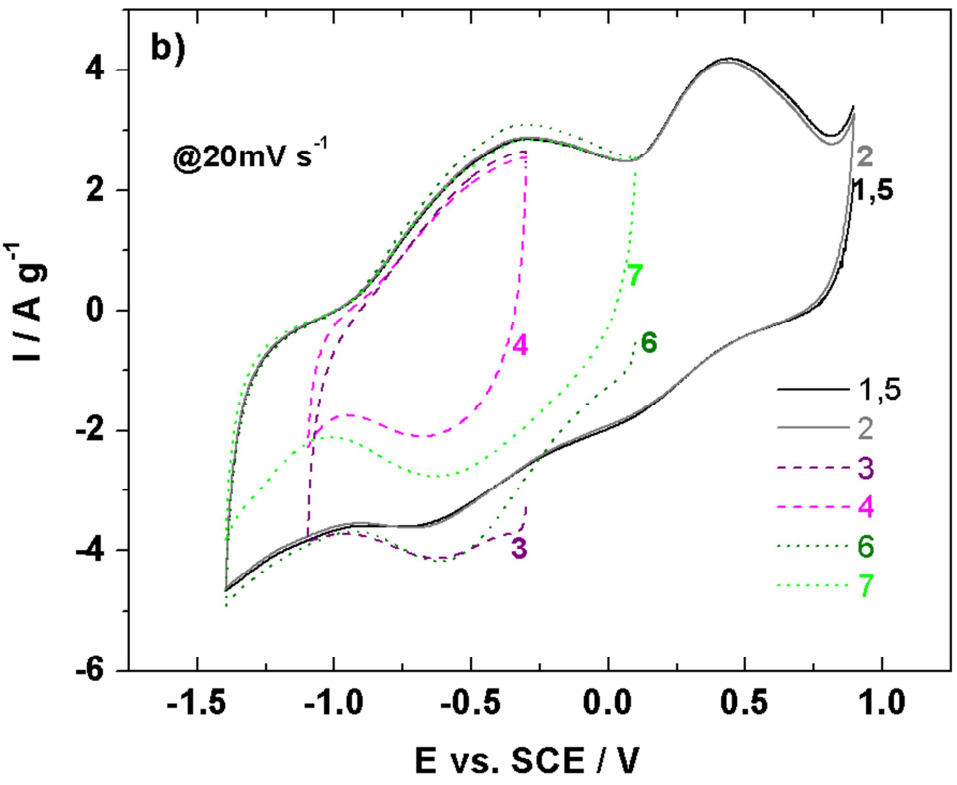

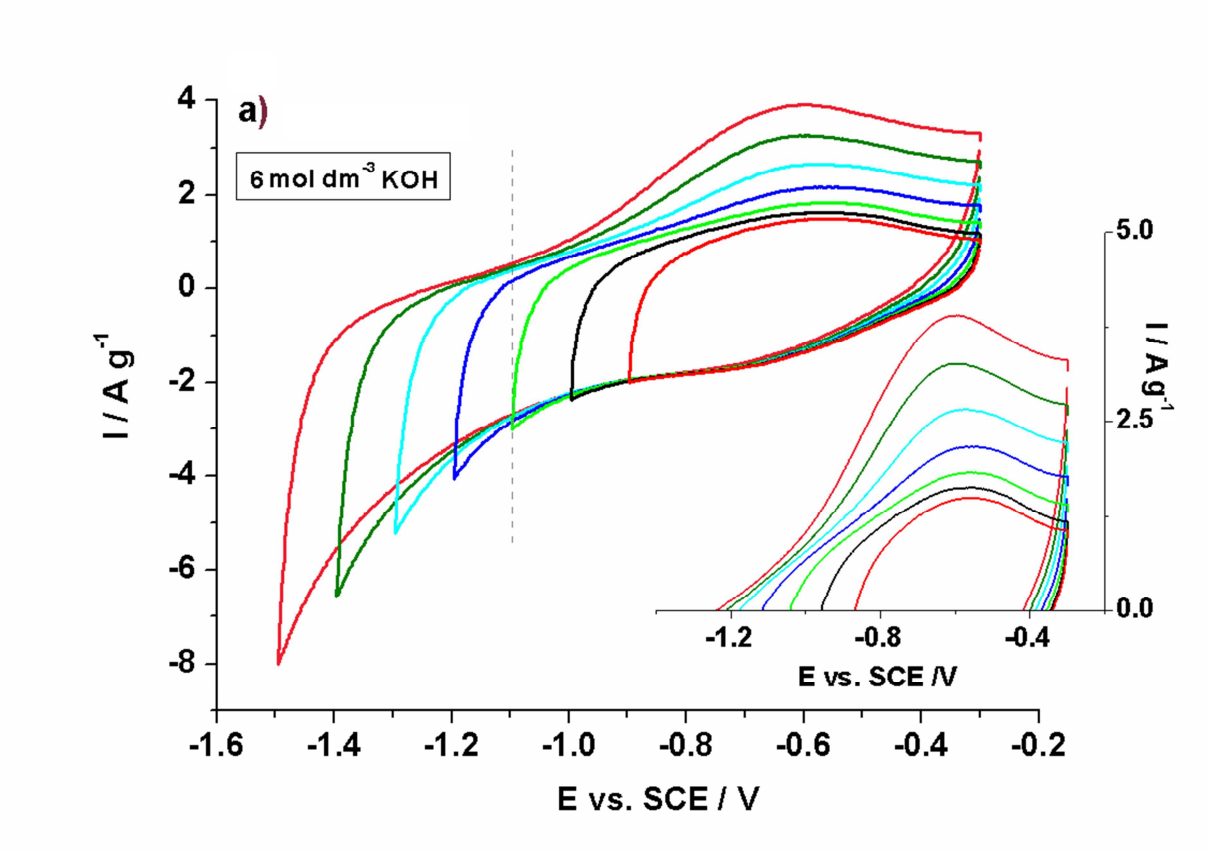

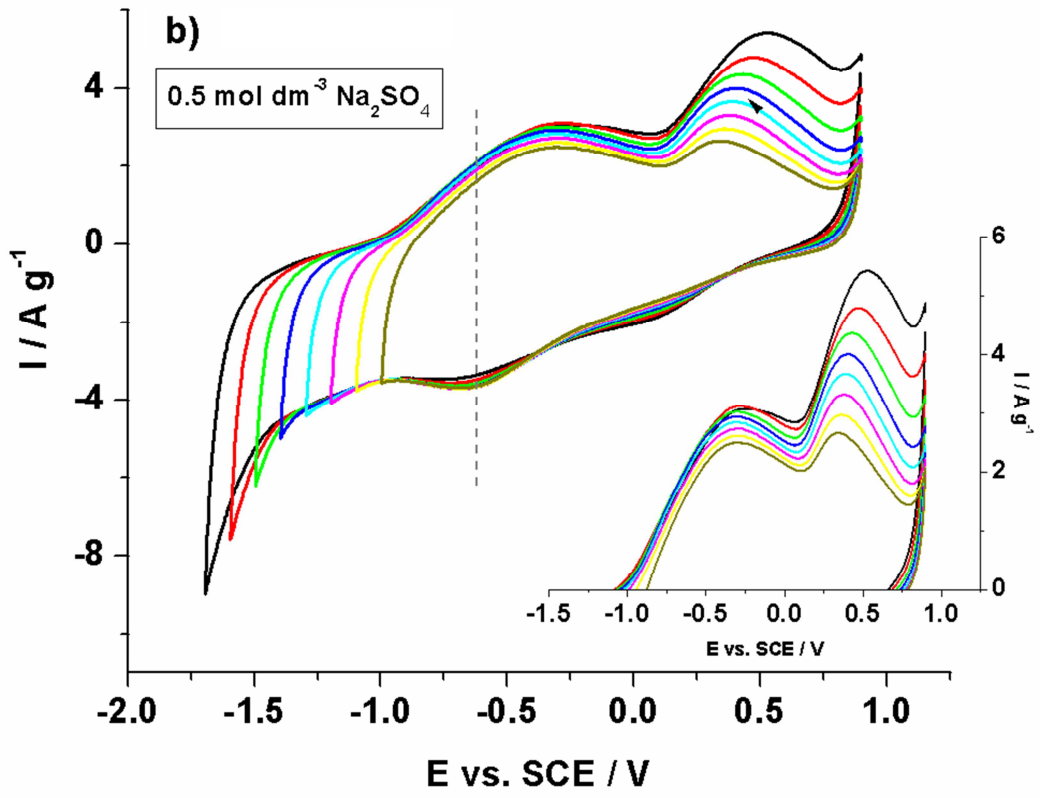

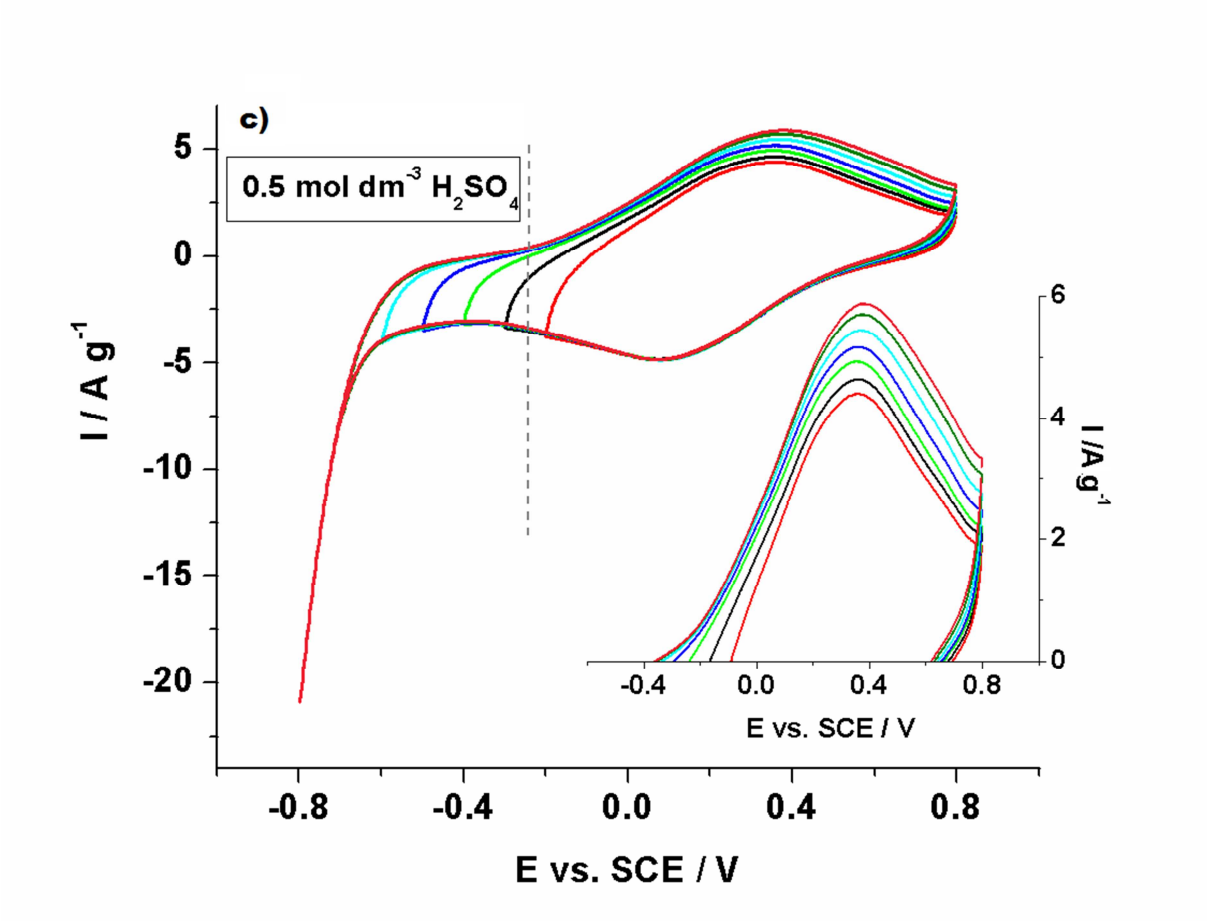

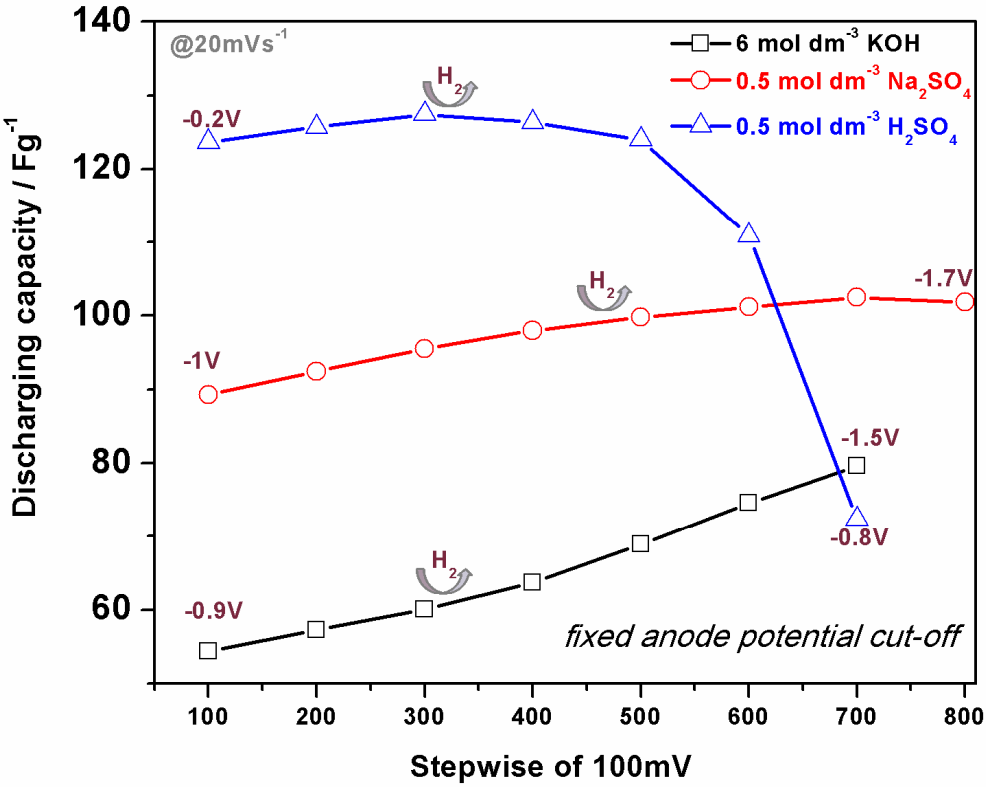

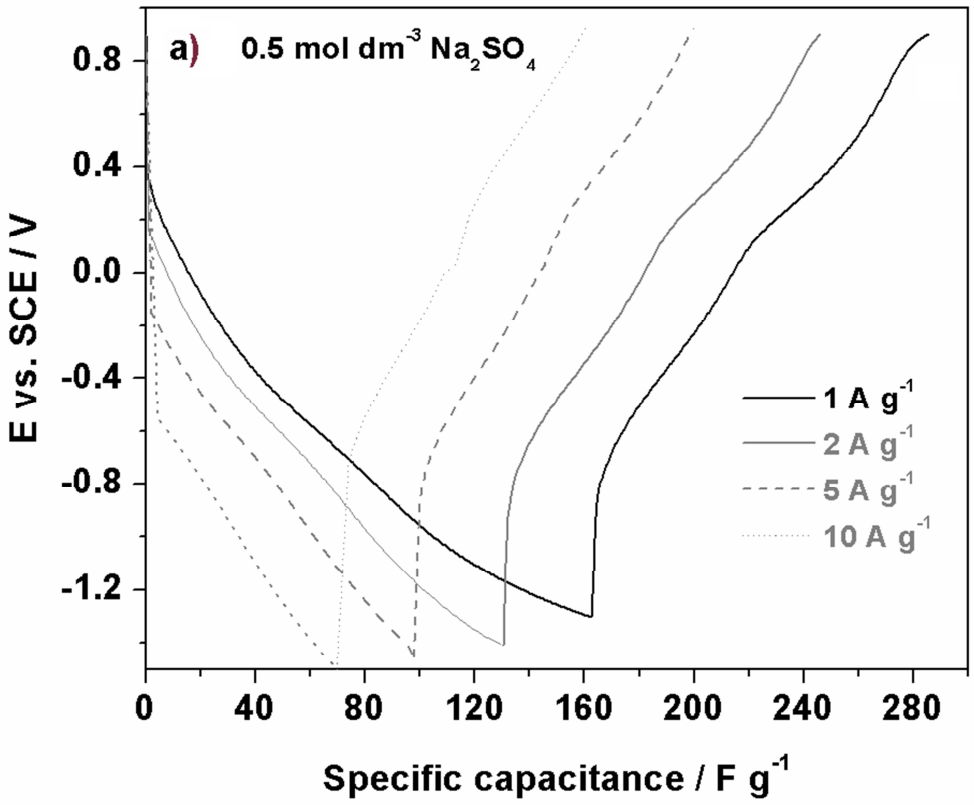

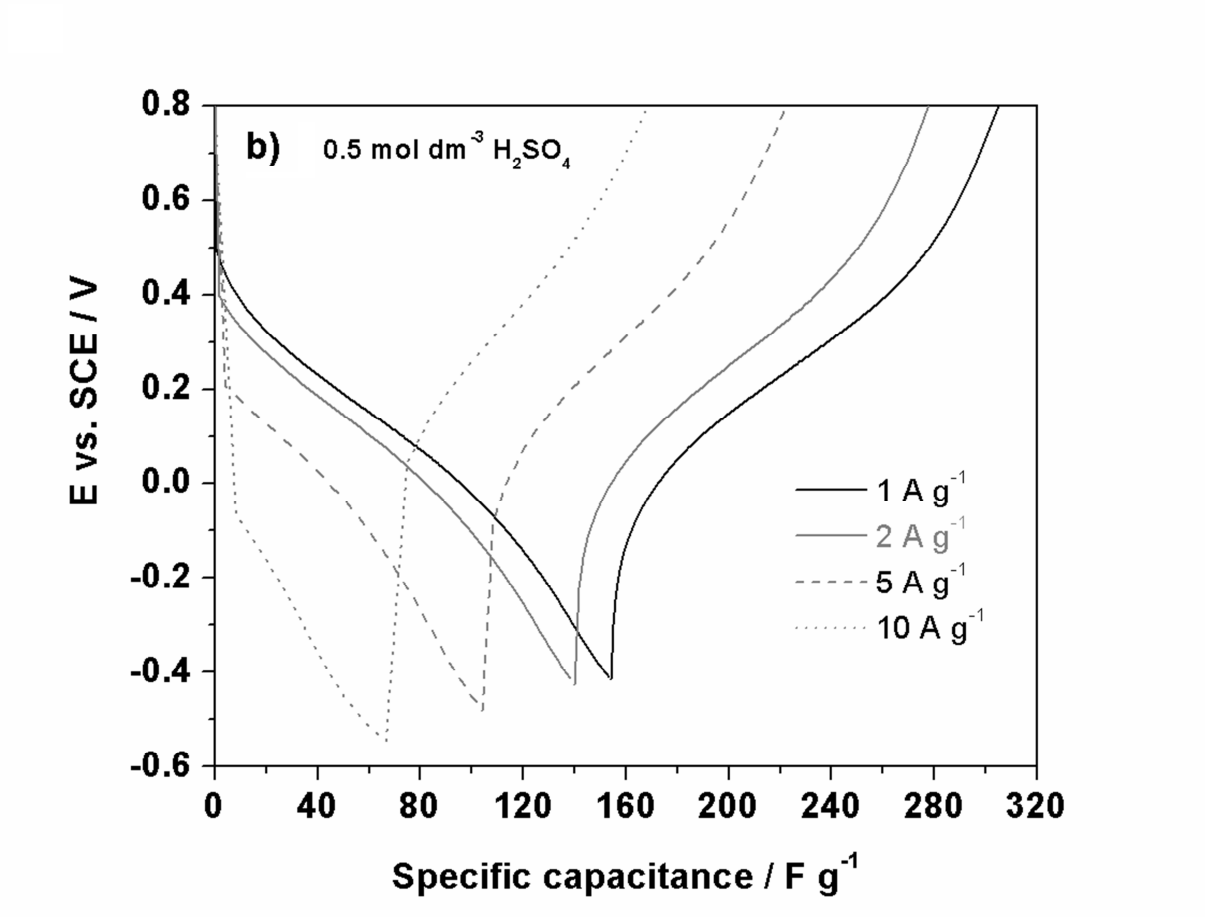

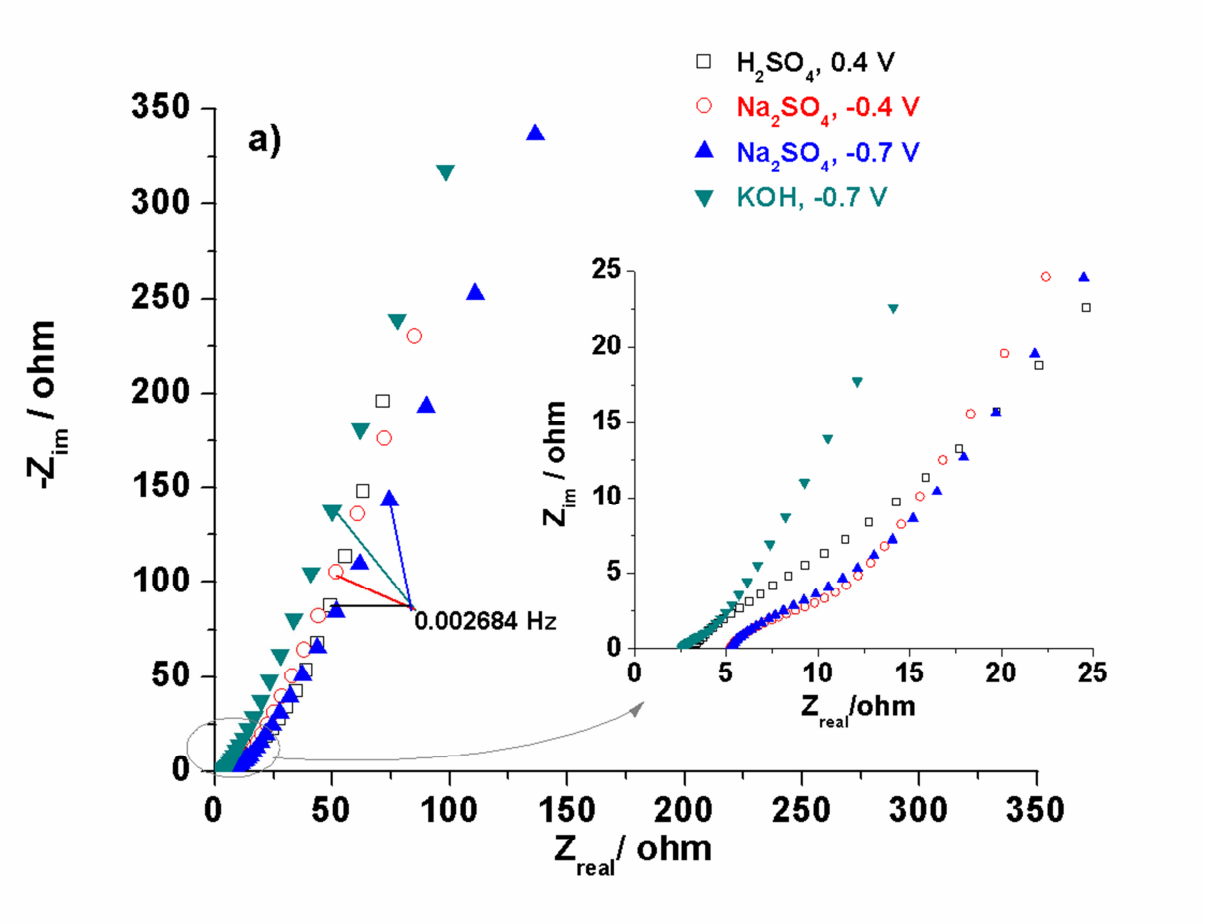

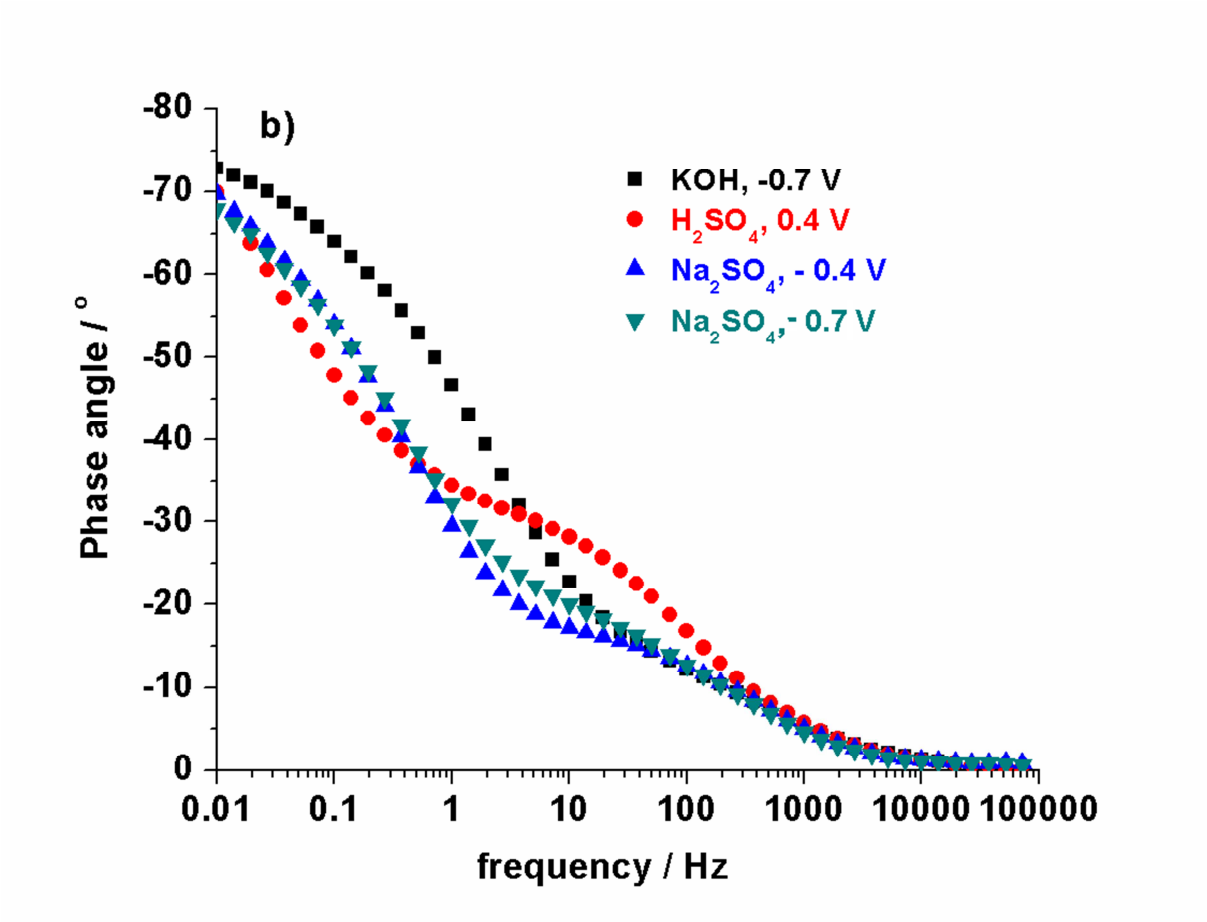

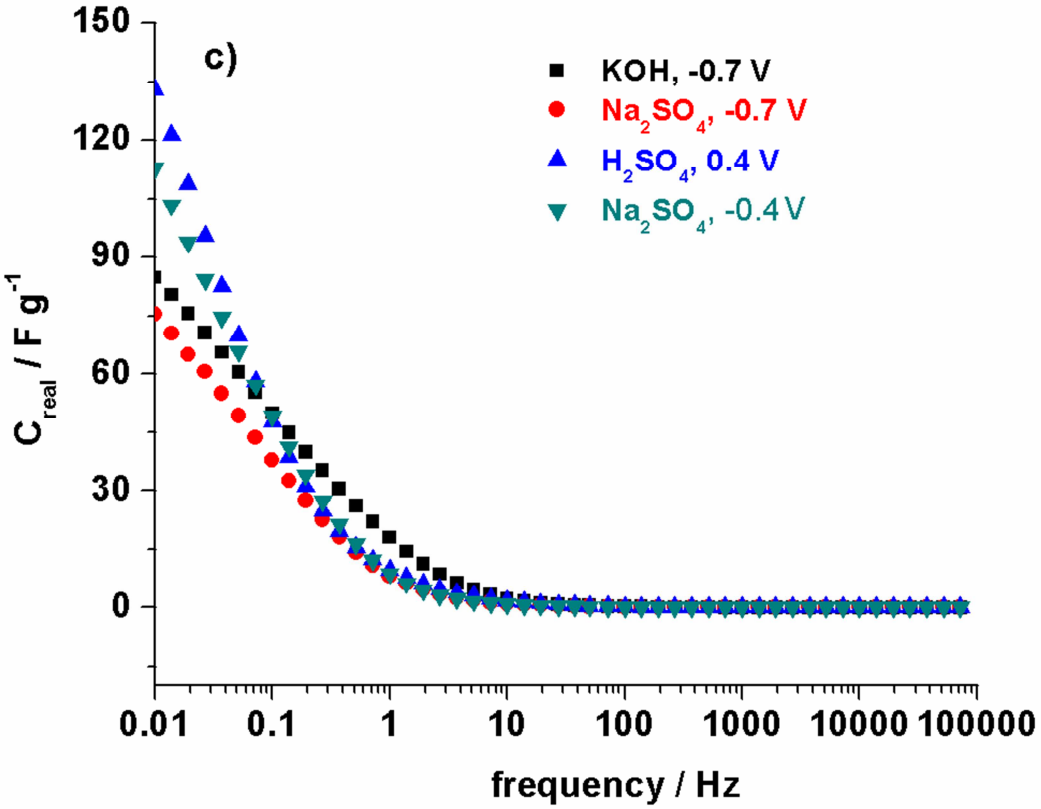

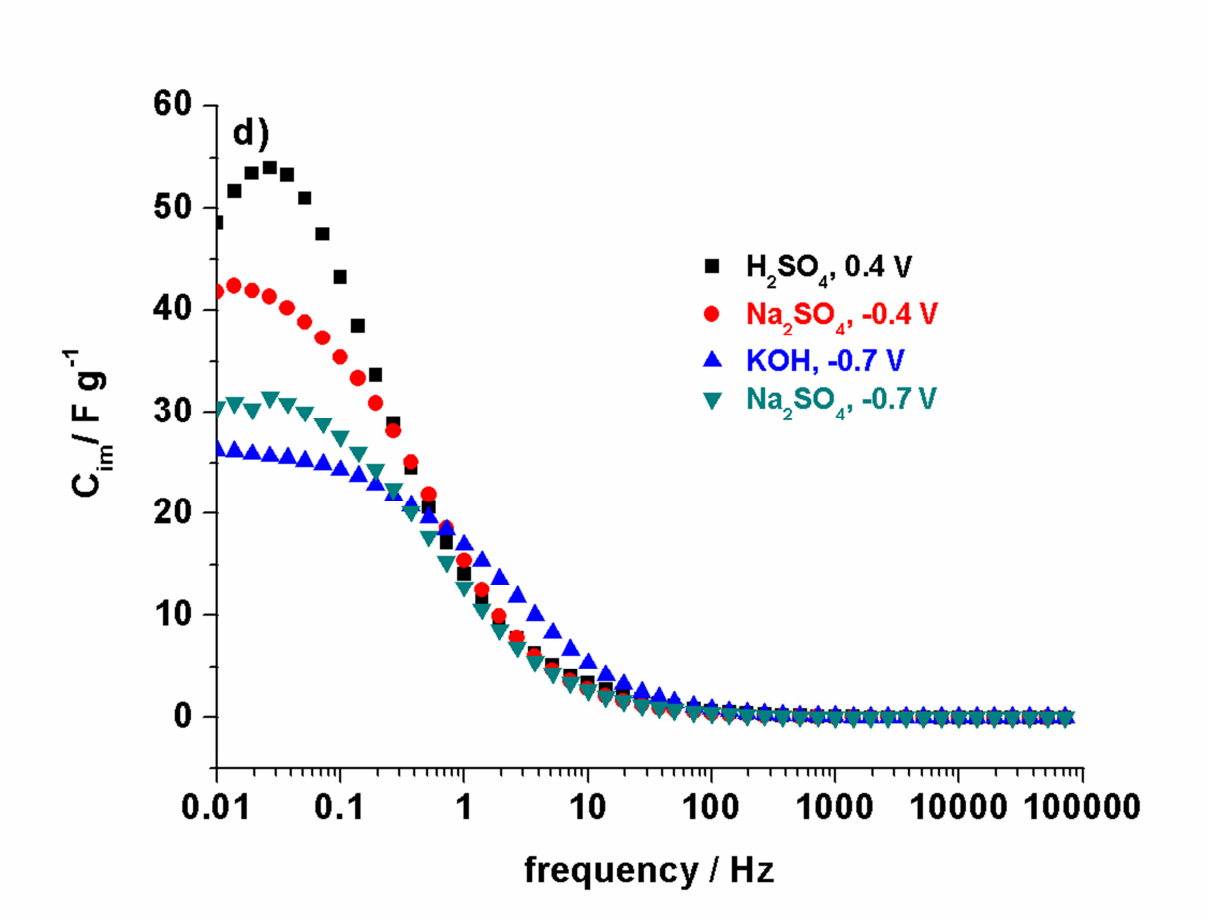

Highlights

- Microporous carbon (ZTC) was synthesized by zeolite Y (Na–form) as a template.
- The charge storage ability of ZTC was detailed studied in various aqueous solutions.
- Pseudo–faradaic reactions of ZTC were observed in neutral electrolytic medium.
- Na_2SO_4 appears as the best choice of aqueous electrolytes for ZTC capacitor.